A unifying explanation of primary generalized seizures through nonlinear brain modeling and bifurcation analysis

Breakspear, M.[1,2,3], Roberts, J.A.[1], Terry, J.R.[4], Rodrigues, S[4], Mahant, N[5], Robinson, P.A.[1,2]

1. School of Physics, University of Sydney, NSW, Australia.
2. Brain Dynamics Centre, Westmead Hospital, Westmead, NSW, 2145, Australia.
3. School of Psychiatry, University of NSW, Randwick, NSW, Australia.
4. Department of Mathematical Sciences, Loughborough University, Loughborough, U.K.
5. Department of Neurology, Westmead Hospital, Westmead, NSW, 2145, Australia

Keywords: Primary generalized epilepsy, neural modeling, nonlinear dynamics, bifurcation, time series analysis

Abstract

The aim of this paper is to explain critical features of the human primary generalized epilepsies by investigating the dynamical bifurcations of a nonlinear model of the brain's mean field dynamics. The model treats the cortex as a medium for the propagation of waves of electrical activity, incorporating key physiological processes such as propagation delays, membrane physiology and corticothalamic feedback. Previous analyses have demonstrated its descriptive validity in a wide range of healthy states and yielded specific predictions with regards to seizure phenomena. We show that mapping the structure of the nonlinear bifurcation set predicts a number of crucial dynamic processes, including the onset of periodic and chaotic dynamics as well as multistability. Quantitative study of electrophysiological data supports the validity of these predictions and reveals processes unique to the global bifurcation set. Specifically, we argue that the core electrophysiological and cognitive differences between tonic-clonic and absence seizures are predicted by the global bifurcation diagram of the model's dynamics. The present study is the first to present a unifying explanation of these generalized seizures using the bifurcation analysis of a dynamical model of the brain.

Introduction

Primary generalized seizures are pathological brain rhythms that, by definition, involve all cortical regions and which are associated with a gross disruption of cognitive activity. Absence (Petit Mal) and tonic-clonic (Grand Mal) seizures are the two main generalized seizures in humans. Several features critically distinguish these two seizure types: Tonic-clonic seizures are associated with markedly different pre- and post-ictal EEG, lengthy duration, and dynamically evolving wave-forms that occur within each seizure. Whilst subjects are typically awake and conscious prior to the seizure, they are invariably unconscious post-ictally. In contrast, Absence seizures have a brief on-off quality, similar pre- and post-ictal EEG and a well structured periodic spike and slow-wave shape which slows only slightly during the seizure but does not significantly alter in its morphology. Remarkably, cognitive function is only minimally disrupted after the seizure. The aim of this paper is to study the mechanisms underlying the onset, evolution and offset of these seizures using a physiologically motivated model of the brain's dynamics. More specifically, we test and extend a number of specific predictions (Robinson *et al.* 2002) based on the premise that generalized seizures represent a transition from stable, linear dynamics to unstable nonlinear behavior by studying the nature of the model's bifurcations. In doing so, we seek a formal and unified explanation of the generalized seizures.

A bifurcation is a sudden change in a dynamical system's activity, such as from steady state to periodic behavior. The transition from laminar to turbulent fluid flow is a well-known physical example. Nonlinear instabilities and bifurcations in large-scale neural activity may be of special significance to brain dynamics: Depending on the context, timing and extent, such phenomenon may be either adaptive – allowing flexible switches in cognitive set (Wright *et al.* 1985, Friston 2000, Breakspear 2002, Freeman & Rogers 2002, Breakspear *et al.* 2003) and behavior (Kelso *et al.* 1992, Fuchs *et al.* 2000, Daffertshofer *et al.* 2000) – or disruptive, such as at the onset of a generalized seizure (Arnhold *et al.* 1999, Stam & van Dijk 2002). Understanding such nonlinear instabilities may provide a unique window into the nature of neurophysiological processes occurring in neural systems since they denote particular types of dynamical processes (Crevier & Meister 1998, Izkehelde 2001), such as those with strong feedback and nonlinearity. Finally, a bifurcation from linear to nonlinear brain dynamics would render any data analysis method grounded in stochastic linear theory problematic. Hence the elucidation of bifurcations in large-scale neuronal systems has cognitive, physiological and methodological significance to neuroscience.

Bifurcations occur in a variety of forms, such as from linear (steady state) to nonlinear dynamics or from one type of nonlinear oscillation to another (Abraham & Shaw 1992). The former can occur if the strength of a feedback process rises above a critical value. Several empirical studies have concluded that large-scale electrical activity in the healthy human brain is, indeed, predominantly a linear/stochastic phenomenon with intermittent instances of weakly nonlinear fluctuations in the alpha frequency (8-13Hz) range (eg. Stam *et al.* 1999, Breakspear & Terry 2002): The nonlinear neural model employed in the present study is able to predict and explain a variety of resting and sleeping state EEG when evolving in a stable, weakly damped linear regime (Robinson *et al.* 2001, 2004). This view (of only occasional and weak nonlinearities) also finds strong support in the success of classic functional neuroscience algorithms which are rooted in a stochastic/linear framework (Friston *et al.* 1994). In contrast, clinical research suggests that several pathological processes, such as seizures (Andrzejak *et al.* 2001) and abnormal rhythms in pathological states (Stam *et al.* 1997a,b) have a strong nonlinear component. In Robinson *et al.* (2002) it was proposed that the transition from resting-state EEG to seizure activity may be viewed as a bifurcation from linear to nonlinear oscillations in the brain's electric activity, whereas different types of seizures may be viewed as bifurcations between distinct types of nonlinear dynamics (see also Wendler *et al.* 2002, Lopes da Silva *et al.* 2003, Perez Valezquez *et al.* 2003).

The present paper undertakes to formally study this hypothesis in a physiologically-based model of brain activity (Robinson *et al.* 2001). Two instabilities are studied – one at approximately 3Hz and the other within the alpha (10Hz) rhythm. These represent the respective frequencies at which Absence and tonic-clonic seizures are initiated. The behavior of the model at and beyond such instabilities is compared to three EEG data sets - one of young subjects with absence seizures, one of tonic-clonic seizures and another of resting state healthy adult subjects. The former two sets allow comparison between modeled and experimental seizure data. The latter data have been previously shown to be associated with weak nonlinear structure (Stam *et al.* 1999, Breakspear & Terry 2002) and hence permit analysis of the model in a stable, resting state - although in the vicinity of an instability. The local bifurcation diagrams are studied for each instability and then compared to the observed phenomena. The global bifurcation diagram – obtained by examining the structure of the bifurcation set under changes in multiple parameters potentially permits local features of each instability to be understood from a global and unifying perspective. We hence investigate whether the topology of the global bifurcation diagram explains the essential difference between absence and tonic-clonic seizures by inter-relating them within this broader framework.

Methods

There are three components to the methodology: (1) The nonlinear corticothalamic model which forms the basis for the bifurcation and time series analysis. A description of this model is given below, and follows Robinson *et al.* (2001, 2002). (2) Scalp EEG data - which permits empirical testing of the predictions generated by the model - is then described. (3) Nonlinear techniques are employed in order to study numerical data generated from the model and the observed scalp EEG data. These are described last.

Corticothalamic brain model

Large-sale neural activity arises from interactions between several neural populations, notably excitatory and inhibitory cortical neurons and specific subcortical nuclei such as the thalamus. The corticothalamic model studied here is based upon the evolution of several dynamical variables within each of these populations. The variables represent the local mean value of a physiological process at position **r** in these neural systems, averaged over a small patch (~0.3mm) of surrounding neuropil. Hence this model belongs to the class of 'lumped' or 'mean field' neural models (Nunez 1974, Freeman 1975, Jirsa & Haken 1996, Robinson *et al.* 1997).

General (spatially continuous) model

We first describe the model in its general form. The dynamical variables within each neural population are the local mean cell-body potentials V_a, the mean rate of firing at the cell-body Q_a, and the propagating axonal fields ϕ_a. The subscript a refers to the neural population (e=excitatory cortical; i=inhibitory cortical; s=specific thalamic nucleus; r=thalamic reticular nucleus; n=nonspecific subcortical noise). The firing rates Q_a are related to the potentials V_a according to the sigmoid activation function $Q_a(\mathbf{r}, t)=\mathrm{S}[V_a(\mathbf{r}, t)]$ where S is a smooth sigmoidal function that increases from 0 to Q_{max} as V_a increases from -∞ to ∞. We model S as

$$\mathrm{S}(V)=\frac{Q_{\max}}{1+e^{-\pi(V-\theta)/\sqrt{3}\sigma}}, \qquad (1)$$

where □ is the mean neural firing threshold, σ is the standard deviation of this (normally distributed) threshold and $Q_{\max}$ is the maximum firing rate.

In each neural population, firing rates Q_a are propagated outwards as oscillating fields ϕ_a according to the damped wave equation

$$D_a\phi_a(\mathbf{r},t) = Q_a(\mathbf{r},t), \tag{2}$$

where the (spatio-temporal) differential operator D_a is given by

$$D_a = \frac{1}{\gamma_a^2}\left[\frac{\partial^2}{\partial t^2} + 2\gamma_a\frac{\partial}{\partial t} + \gamma_a^2 - v_a{}^2\nabla^2\right]. \tag{3}$$

The parameter $\gamma_a = v_a/r_a$ - where r_a and υ_a are the characteristic range and conduction velocity of axons of type a - governs the dispersion of propagating waves. ∇^2 is the Laplacian operator (the second spatial derivative). The system of equations is closed by introducing the effect of incoming axonal inputs to neurons at **r** from other neural populations. The cell body V_a results after post-synaptic potentials have been filtered in the dendritic tree and then summed. For excitatory and inhibitory neurons within the cortex, this is modeled using a second order delay-differential equation (Robinson *et al.* 2001),

$$D_\alpha V_a(\mathbf{r},t) = v_{ae}\phi_e(\mathbf{r},t) + v_{ai}\phi_i(\mathbf{r},t) + v_{as}\phi_s(\mathbf{r},t - t_0/2), \tag{4}$$

where $a=e,i$ and the (temporal) differential operator, given by

$$D_\alpha = \frac{1}{\alpha\beta}\frac{\partial^2}{\partial t^2} + \left(\frac{1}{\alpha} + \frac{1}{\beta}\right)\frac{\partial}{\partial t} + 1, \tag{5}$$

incorporates dendritic filtering of incoming signals. The quantities α and β are the inverse rise and decay times of the cell body potential produced by an impulse at a dendritic synapse. Note that input from the thalamus to the cortex is delayed in (4) by a propagation time $t_0/2$. For neurons within the specific and reticular nuclei of the thalamus it is the input from the cortex which is time-delayed and hence

$$D_\alpha V_a(\mathbf{r},t) = v_{ae}\phi_e(\mathbf{r},t - t_0/2) + v_{as}\phi_s(\mathbf{r},t) + v_{ar}\phi_r(\mathbf{r},t) + v_{an}\phi_n(\mathbf{r},t), \tag{6}$$

where $a=s,r$. The synaptic strengths are given by $v_{ab}=N_{ab}S_b$ where N_{ab} is the mean number of synapses from neurons of type b to type a and S_b is the strength of the response to a unit signal from neurons of type b. The final term on the RHS permits ascending stochastic input from the brainstem: To simulate a real physiological

system, this term is noise modulated for the time series illustrations. However, for the bifurcation diagrams the term is constant. The default values of all parameters are given in Table 1. All parameter values chosen in this study have been employed in previously published studies (Robinson *et al.* 2002), emphasizing that the results of the numerical analysis are used in a predictive rather than exploratory vein in relationship to the EEG data.

Setting all spatial and temporal derivatives in (1)-(6) to zero determines global (spatially invariant) corticothalamic steady states. Small perturbations around these states (representing noisy influx from the brainstem) obey a linear wave equation, the study of which has been employed to explain resting state EEG temporal (Robinson *et al.* 1997, 2001, 2004) and spatial (O'Connor *et al.* 2002) spectra. We use a 2-D cortex and a standard first order approximation to ∇^2 (Abramowitz & Stegun 1970).

Global (spatially invariant) model

A full nonlinear analysis of this system is a highly nontrivial task. However, in certain circumstances, particularly in the study of generalized seizures, brain activity may be dominated by very large scale – or even whole brain – processes, in which case the dynamical variables may not depend greatly on spatial position **r.** This 'global model' can be studied by setting the spatial gradient term in equation (3) to zero, yielding

$$D_a = \frac{1}{\gamma_a^2}\left[\frac{d^2}{dt^2} + 2\gamma_a \frac{d}{dt} + \gamma_a^2\right]. \qquad (7)$$

The variables V_a, Q_a and ϕ_a now depend solely on t and not **r**. The smallness of r_i also let's us set $\gamma_i \approx \infty$, yielding a set of seven first order delay-differential equations. These equations permit a computationally parsimonious method of studying large-scale brain dynamics and are employed for the majority of the present study. They are given in Appendix A1.

Studying the linear stability criteria for this system permits mapping of the boundary which marks the transition between steady state behavior and nonlinear oscillations. Previous exploration of the model for realistic parameter ranges revealed a small number of key instabilities which constrain the way nonlinear oscillations may arise (Robinson *et al.* 2002). As well as the 3Hz and alpha instability studied in the present study, slow wave (<1Hz) and spindle instabilities (approx. 12Hz) may also arise. The occurrence of only a small number of instabilities suggests that it may also be possible

to study the dynamics and stability of the brain in a phase space of low dimensionality. Indeed, formal analysis of low frequency instabilities suggests that three variables x, y and z – parameterizing corticocortical, corticothalamic and intrathalamic instability – fully capture the parameter combinations at which the brain model loses stability (Robinson *et al.* 2002). These combine dynamic variables and state parameters and are given in Appendix A2. They enable visualization of where in parameter space the model becomes unstable. In Fig. 1 the instability boundary within this truncated space is presented. The zone within the tent-shaped region is associated with stability of the model, whereas points outside are associated with nonlinear oscillations. The bifurcation diagram studied in further detail below includes this "tent diagram" (Robinson *et al.* 2002) plus further information concerning transitions between different types of nonlinear oscillations.

In the present study, the general model is only required in the section dealing with weak nonlinear interdependence in the resting state data. The spatially invariant model is employed to study the onset of the generalized seizures. Numerical integration was performed using a fourth order Runge-Kutta integrator. A cubic-spline interpolator was employed in order to estimate the time delayed values of the midpoints required for the Runge-Kutta algorithm.

Scalp EEG Data

Three EEG data sets are studied. All are scalp EEG data with electrode placement following the 10-20 international system and linked earlobe reference. Ethics approval was obtained prior to data collection for each data set, according to the Ethics Committee at each Institution.

1. *Healthy human EEG alpha data* collected from 40 adults (age 20-54) who disavowed psychiatric or neurological illness at Westmead Hospital, Sydney. Skin resistance at each site was < 5 kΩ. Data was collected at a rate of 250 Hz through a SynAmps^{TM} amplifier and filtered with a 50 Hz low-pass third order Butterworth filter. Artifacts caused by eye movement were corrected offline according to the method of Gratton *et al.* (1983). Data was collected from each subject during 130 s of a resting eyes-open paradigm, and 130 s during a resting eyes-closed paradigm.
2. *Absence seizure data* drawn from a database of thirteen adolescent epileptic patients in the department of Neurology, Westmead Hospital, Sydney. Data was collected at a rate of 200Hz and filtered with a 70 Hz low-pass filter.
3. *Generalized tonic-clonic seizure data* drawn from a data base of seven epileptic patients (Quian Quiroga *et al.* 2002). These patients were admitted to

an epilepsy monitoring unit with diagnosis of pharmacoresistant epilepsy and no other accompanying disorders. Antiepileptic drugs (AEDs) were gradually tapered after admission. Each signal was digitized at 409.6 Hz through a 12 bit A/D converter and filtered with an "antialiasing" eight pole lowpass Bessel filter with a cutoff frequency of 50 Hz. The signal was digitally filtered with a 1-50 Hz bandwidth filter and stored at 102.4 Hz. The scalp recording was measured bipolarly from the T4-T6 (right temporal) locations.

Nonlinear Data Analysis

EEG data

In order to test whether seizure activity is associated with nonlinearity – implicit within the hypothesis that a seizure occurs after a nonlinear bifurcation - a nonlinear prediction algorithm (Casdagli 1989) was employed. Briefly, the data is divided into discrete time windows. In each window a "nonlinear prediction error" is calculated. This error reflects the ability of a local nonlinear model to predict the amount of uncertainty in the data. Low errors indicate a good fit and hence nonlinear structure. Using a bootstrap or resampling scheme (applied to the original data), an ensemble of prediction errors is then calculated to represent the null hypothesis that the values of the errors are due to purely linear correlations within the data (Theiler *et al.* 1992). The data is said to contain nonlinear structure if the observed (experimentally derived) prediction error lies outside of the distribution of these "surrogate" errors (for further details see Terry & Breakspear 2003). Nineteen surrogates were constructed to allow for non-parametric statistical inference at 95% confidence within each window. For graphical clarity, the inverse of the prediction errors – which we denote the 'nonlinear prediction indices' – are plotted in the Results.

A modification to this algorithm allows multichannel EEG data to be tested for evidence of nonlinear interdependence - a nonlinear equivalent to the coherence function (Schiff *et al.* 1997, Terry & Breakspear 2003). A multivariate surrogate algorithm (Prichard *et al.* 1994, Rombouts *et al.* 1995) is then employed to exclude the contributions of purely linear correlations. This can be used in conjunction with the spatially discrete version of the corticothalamic model to estimate the predicted nonlinear contribution to spatiotemporal patterns within brain activity.

Numerical data

Bifurcation diagrams visualize sudden changes in a dynamical system subsequent to incremental changes in a state parameter. In order to construct these, numerical integration was performed across a varying range of v_{se} - the excitatory influence of cortical pyramidal cells onto the specific thalamic nuclei. This parameter was chosen because of its simple physical meaning and the prior implication of excitatory corticothalamic feedback in the pathophysiology of generalized tonic-clonic (Zifkin & Dravet 1997, McCormick & Contreras 2001) and absence (Destexhe & Sejnowski 2001, McCormick & Contreras 2001, Meeren *et al.* 2002) seizures. Local maximums and minimums of the resulting numerical time series are plotted for each parameter value. For the time series comparison of the model and EEG data, we plot the macroscopic excitatory field potentials ϕ_e as these best represent the cortical correlate of scalp potentials up to a linear transformation of the amplitudes (Nunez 1995). Specifically, scalp potential is proportional to the cortical potential, which is proportional to the mean cellular membrane currents, which are in turn proportional to the firing rates. Hence, apart from a (dimensional) constant of proportionality, and the effects of volume condition scalp EEG signals correspond closely to ϕ_e (Robinson *et al.* 2004). Parameter values are given in Table 1. To better simulate a real physiological system, small amplitude (SNR=0.90) autocorrelated stochastic terms were added to the parameters (system noise) for the numerical time series plots. Such noise was generated according to,

$$s(t_n) = \rho s(t_{n-1}) + \sqrt{1-\rho^2}\, r(t_n), \tag{8}$$

where $r(t)$ is drawn from of a set of zero mean independent random numbers, $s(t_0)=r(t_0)$ and the desired autocorrelation factor t_c between adjacent time steps is given by,

$$t_c = -\Delta t \Big/ \ln(p). \tag{9}$$

Such a model of parameter noise represents the simplest method of simulating an autocorrelated stochastic process. It should be noted that such noise is only used in the time series plots and has no impact on the calculation of the model's bifurcation diagram.

Results

The analysis of the results is presented in three sections: (1) The bifurcation occurring at the 3 Hz instability is first studied as a model for Absence seizures. The analysis of

the model is given first, permitting prediction of the electroencephalographic data which follows. (2) The alpha instability is then presented. In order to underline that the model predicts the emergence of seizure activity from resting state data, and because previously published data is available, we first present an analysis of the model very close to the alpha instability – a "weak" instability. Subsequently, we present the full bifurcation of the global model to predict generalized tonic-clonic seizures. As with the 3 Hz instability, the model and then the EEG data are studied. (3) The global bifurcation is then presented in order to permit potential unification of the 3Hz and alpha instabilities.

Absence seizure: Corticothalamic model

We first study the nonlinear instability occurring at approximately 3 Hz. This is achieved by choosing physiologically plausible parameters which place the system in the vicinity of a weak 3Hz instability (Robinson *et al.* 2002) as given in Table 1. As stated above, v_{se} is then varied in order to study the geometry of the bifurcation set.

The results are presented in Fig. 2. The bifurcation diagram - Panel (a) - exhibits a Hopf bifurcation to periodic dynamics with an initial (supercritical) instability at v_{se} $\approx 1.8 \times 10^{-4}$ Vs and further period-doubling instabilities at v_{se} $\approx 3.4 \times 10^{-4}$ Vs and v_{se} $\approx 4.2 \times 10^{-4}$ Vs. In this noise-free plot, it can be seen that only periodic oscillations occur. An exemplar time series, with added system and measurement noise is given in Panel (b). This was created by dynamically ramping v_{se} from the linearly stable (weakly damped region) upwards into the region of linear instability (Panel c). The dashed lines in Panel (a) show the extreme values of the ramp function. Close-up images of the onset (Panel d) and offset (Panel e) of the seizure exhibit a number of key phenomena: (1) Shortly after the onset of ramp-up of v_{se} at t=5 s periodic oscillations of growing amplitude appear in the field potentials. These occur as the system passes through the periodic regime in the bifurcation plot. (2) After two to three cycles, spike and slow-wave oscillations appear, heralding the onset of period doubling limit-cycle oscillations. These continue throughout the seizure, although their amplitude is modulated by the combined effects of system and measurement noise. (3) During the ramping down of v_{se} at t=19.5 s the amplitude of the spike and wave oscillations diminish. The spikes disappear at approximately t=20.5 s as the system passes through the simple period-one regime. (4) Finally, the remaining oscillations are damped away and the system returns *directly* to the same preictal EEG state, governed by stable damped stochastic fluctuations. This is reflected in the spectrum of the seizure (Panel f), showing similar pre- and post-ictal spectra. The

seizure spectrum is dominated by the 3 Hz spike and wave oscillation and its harmonics.

A (three dimensional) time-delay embedded phase portrait of a simulated (noise-free) seizure is shown in Panel (g). Grey arrows indicate the flow of orbits away from the unstable fixed point subsequent to the bifurcation and onto the limit cycle attractor. The growth in amplitude of the spike (at the far side of the attractor) can be seen as the orbits spiral outwards. The orbits follow the same unstable manifold (but spiraling downwards) at the conclusion of the seizure (not shown). Panel (h) depicts the morphology of the seizure in the space spanned by the corticocortical, corticothalamic, and intrathalamic "stability" variables, x, y, and z. As expected, the seizure is located outside the tent-shaped stability zone. Because the seizure corresponds to limit cycle dynamics, it can be embedded within this three dimensional space without crossing of the orbits (i.e. with uniqueness of the solution curves). This indicates that, during such a seizure, a dynamical system of reduced dimensionality should be able to sufficiently describe the macroscopic neural dynamics – or, equivalently, a relatively small number of physiological processes may be responsible for the onset and maintenance of the seizure activity.

Panel (i) shows the spike and slow wave morphology of the three principal fields plotted together (cortical excitatory-solid, specific thalamic-dotted and reticular thalamic-dashed). It should be noted that such behavior occurs after two period doubling bifurcations have occurred: Hence the above dynamics reflect a period-4 oscillation. Because of this, two full "circuits" through the corticothalamic loop are required in order to complete a full Absence waveform. Further simulations within the parameter space of 3 Hz nonlinear oscillations yield a variety of spike and wave and poly-spike morphologies. The exact wave form is sensitive to changes in the state parameters, possibly accounting for the between-subject variance of Absence waveforms. This illustration reveals the potential of a corticothalamic model to elucidate the mechanisms and sequence of events leading to epileptic waveforms. Although a spike may be most apparent firstly in the reticular nucleus in this realization, the existence of a spike is an emergent phenomenon of the corticothalamic system in the current parameter regime – that is, on a period-two limit-cycle attractor. The exact mechanisms of spike formation within this system are beyond the scope of the present study.

Absence seizure: Scalp EEG data

The first step of the experimental EEG data analysis was to test the key premise of the paper, namely that seizures correspond to bifurcations from linearly stable to nonlinear oscillations. As discussed above, this was achieved by using a measure of nonlinear predictability and comparing EEG to phase-randomized surrogate data. An exemplar Petit Mal seizure (F_z electrode) is shown in Fig. 3, Panel (a). In Panel (b), the normalized predictability index is given as the solid line. Plots obtained from 19 surrogate sets are dashed lines. It can be seen that the occurrence of the seizure is coincident with a sudden and large increase in this index of nonlinear structure, consistent with the appearance of nonlinear oscillations. Also noteworthy is that the pre- and post-ictal EEGs are associated with intermittent and weak nonlinearity, evident as occasional increases in the nonlinear predictability of the real compared to the surrogate data (arrows). This is consistent with noisy perturbations of a weakly damped nonlinear system. In other words, pre- and post-ictal states represent a system close to a bifurcation. Comparable results were observed for all Petit Mal seizures studied.

Panels (c) and (d) illustrate an example of a numerically simulated Petit Mal seizure, integrated over a comparable time frame to the real seizure. Because the seizure was generated by pushing the system briefly through nonlinear bifurcations, it is not surprising that a transient increase in nonlinear structure is seen. Prior to, and following, the seizure the system has been set just below the Hopf bifurcation (see Fig. 2a). Hence, the occasional slight increases in nonlinear structure in the model over the surrogate data time series (arrows) during these times are to be expected, when fluctuations toward the bifurcation occur.

The nature of the nonlinear oscillations in the Petit Mal seizure, their growth and decay is studied in Fig. 4. Panel (a) shows a complete seizure, revealing an approaximately symmetrical appearance. The spectrum of this seizure (Panel b) is dominated by the 3 Hz spike and wave morphology. Notably, the post-ictal spectrum returns rapidly to its featureless pre-ictal form. In Panels (c) and (d) the onset and offset of simple periodic, then spike and wave oscillations are clearly visible. A time-delay embedded reconstruction of this seizure is given in Panel (e). The seizure onset (t=3 s to t=5.8 s) is given in blue and the remainder of the seizure (t=5.8 s to t=19.5 s) in black. This plot directly illustrates the outward periodic spiral (blue) of the system onto a large amplitude oscillatory ‘attractor’, comparable to Fig. 2 Panel (g).

It finally remains to determine the nature of the oscillations during the seizure. We refrain from calculating dynamic ‘invariants’ such as Lyapunov spectra, as these are notoriously unreliable in short, noisy time series data (Dammig & Mitschke 1993).

Rather, we study the first-return map, which is an assumption-free method of visualizing the nature of oscillatory dynamics (Perez Valezquez *et al.* 2003). Briefly, level crossings of a dynamical variable are noted. Denote the temporal period between successive crossings as T_n. The graph of T_n against T_{n-1} gives a truncated representation of the full dynamics. A plot of the seizure in Panel (a) is given in Panel (f). For ease of interpretation we plot $f_n=1/T_n$ - the point-wise frequency of the system. The first feature to be noted is that the points fall close to the line $f_n=f_{n-1}$. That is, the system is nearly periodic (the level crossing was chosen below the spike so that in effect we produce a second-return plot – i.e., a true full period of the oscillation). As the arrow denotes, the frequency starts above 3 Hz and quickly falls to approximately 2.6 Hz. It then varies around 2.6 Hz in a manner without any obvious geometrical structure – that is, not confined to any obvious low-dimensional invariant. We interpret this as the noisy modulation of a fixed point in this plot – that is, a noisy limit cycle of the full dynamics. This is consistent with the findings of a purely empirical study using a different methodology (Feucht *et al.* 1998).

In summary, the evolution of this seizure quantitatively matches that of the numerical seizure generated by the corticothalamic model in a number of crucial aspects, namely the simple period-doubling manner of onset and offset, the similar pre- and post-ictal spectra and the period (two) nature of the full seizure. The bifurcation plot of Fig. 2a explains these phenomena.

"Weak" nonlinear alpha instability

Previous analysis of scalp EEG data revealed an increase in amplitude and sharpness of the alpha peak during the instances of nonlinear interdependence (Breakspear & Terry 2002). Empirical studies alone, however, are unable to test competing explanations for this phenomenon whereas the current model permits its explicit investigation. The system parameters are first chosen to yield resting state eyes closed dynamics, using previously published parameters (Robinson *et al.* 2002), to yield a strongly damped, stable state. Increasing v_{se} towards (but not beyond) the linear instability boundary yields a very weakly damped, marginally stable system. Comparing the spectral plots of the model in these two states to previously published empirical data investigates whether the resting brain functions in the vicinity of a 10 Hz nonlinear 'corticothalamic' instability. The results are presented in Fig. 5.

The empirical results from the database of healthy subjects' EEG recordings are presented in Panels (a)-(d). Panel (a) shows a pair of bipolar derivations (O_1-P_3 and O_2-P_4) that exhibit strong nonlinear interdependence according to the nonlinear

prediction algorithm discussed above. Panel (b) shows data that do *not* exhibit such a property. Note the 'cleaner', higher-amplitude alpha oscillations of (a) compared to (b). Panels (c) and (d) show the linear and nonlinear properties of these epochs: In (c) is shown the cross-spectral density plots of all epochs showing nonlinear interdependence (solid) compared to those that do not (dashed). The increased amplitude and sharpness of the alpha peak of the 'nonlinear' epochs is clearly visible. Panel (d) shows the 'nonlinear interdependence' prediction errors ∇^H plotted against the length of the forward prediction iteration H, for the EEG data (solid lines with crosses) compared to an ensemble of 19 'surrogate' data (dashed line). Lower prediction errors correspond to stronger nonlinear interdependence. The plain solid line denotes the boundary of the null (purely linear) distribution, defined as the minimum of the surrogate data. The data pair in Panel (a) yielded the lower prediction curve, consistent with strong nonlinear interdependence. The pair in (b) crosses into the null distribution after 6 time-steps and is hence classified as containing only linear cross-dependence (the root-mean-square of the twenty prediction errors is within the root-mean-square of the surrogate distribution).

The corresponding plots for the corticothalamic model are shown in Panels (e)-(h). Setting v_{se}=10.4x10^{-4} Vs places the system close to the alpha instability (see below) and yielded data as shown in Panel (e), which exhibits the same waveform as the 'nonlinear' scalp data of Panel (a). In comparison, v_{se}=10.1x10^{-4} Vs places the system further from the instability, hence ensuring strong damping of any nonlinear perturbations. This yields the noisier data of Panel (f). Comparing the linear cross-spectra of these data (Panel g) reveals the same increased amplitude and sharpening of the alpha peak derived from the weakly nonlinear data (solid) compared to the strongly damped data (dashed). The nonlinear interdependence prediction plots are given in Panel (h). The 'weakly nonlinear' time series in (e) clearly exhibits nonlinear interdependence (solid line with crosses) as the prediction errors are consistently smaller than their surrogate counterparts. The strongly damped epoch (solid line with stars) yields prediction errors well within the null distribution.

Tonic-clonic seizure: Corticothalamic model

We now study the nonlinear dynamics that follow the instability occurring at approximately 10 Hz. This is achieved by increasing v_{se} from that studied in the last section. The results are presented in Fig. 6. Bifurcation diagrams are given for both the macroscopic field potentials ϕ_e (Panel a) and for the pyramidal cell potential V_e (Panel b) as the latter reveal additional dynamical structure. Both of these show a

region of bistability from $\mu_{se} \cong 9.5 \times 10^{-4}$ to $\mu_{se} \cong 10.35 \times 10^{-4}$ Vs. To illustrate this, we first plotted the bifurcation from left to right in black and then from right to left in red. A "continuation technique" is employed whereby the final system values from a previous parameter value are used as the initial conditions when that parameter is changed (either up or down). Hence the region of bistability is revealed when both red and black solutions can be viewed separately. Otherwise black solutions are overlaid by red.

What are implications of this bistable region for the dynamics? An exemplar numerical time series is given in (c). The corresponding values of v_{se} are given in (d). The system is initialized on the linearly stable (black) arm within the bistable zone, close to the linear instability $v_{se} \cong 10.2 \times 10^{-4}$ Vs. Next, v_{se} is increased to $v_{se} = 10.45 \times 10^{-4}$ Vs. The system bifurcates from the fixed point at $v_{se} \cong 10.3 \times 10^{-4}$ Vs (Arrow 1). At this point, the fixed point becomes an unstable spiral and the orbits hence grow exponentially in amplitude (Panel f), reaching the large amplitude attractor seen to the right of the instability. The structure of V_e reveals that this is a period 6 attractor. If v_{se} is then decreased (Arrow 2), the system does not become immediately unstable, but rather tracks back through parameter space on this large amplitude attractor. This explains the ongoing existence of large amplitude oscillations in the time series. When $v_{se} < 9.8 \times 10^{-4}$ Vs the attractor does again become unstable and the orbits collapse back onto the fixed point (Arrow 3). Although the system is back on the fixed point attractor, it has reached this state in quite a different (more strongly damped) region than its initial configuration: In order to return to the original state, it is necessary for v_{se} to be increased again to $v_{se} = 10.25 \times 10^{-4}$ Vs.

This 'loop' through parameter space creates a distinctive fingerprint in the spectral plot (Panel e). Prior to the onset of the seizure, the spectrum displays the characteristic alpha peak of resting state EEG. The power within this peak increases after the bifurcation has been passed, and as the orbits grow exponentially toward the large-amplitude attractor. This power is particularly strongly expressed during the seizure. Due to the nonlinear nature of the oscillations, higher order harmonics (at 20 Hz, 30 Hz, 40 Hz, etc) are clearly evident. Due to the bistability, this pattern remains evident even though v_{se} is dropping below its initial value (Panel d). Once $v_{se} < 9.8 \times 10^{-4}$ Vs, the attractor loses stability and the system returns to the stable linear regime. However, because of the strong nonlinear damping, the overall spectral power is much diminished. Note that power across all frequencies is lower and the alpha peak is absent. The characteristic alpha peak returns when v_{se} is restored to its initial value (10.25×10^{-4} Vs).

Figure 6 (g) shows the large amplitude attractor (in black) that occurs when v_{se} is increased across the bifurcation point. The red orbits show the exponential growth in amplitude towards this attractor once the fixed point has become unstable. In (h) the attractor is depicted again in relationship to the tent-shaped stability zone in the truncated space spanned by the stability variables, *x, y* and *z*. For this panel, all (system and parameter) noise has been with-held, revealing a periodic underlying attractor. An additional feature of the spectral plot (e) during the seizure, most notable at higher frequencies (e.g. between 40 and 50Hz) is the existence of subharmonics at approximately 1/3 and 2/3 of the fundamental frequency. This reflects the period 6 character of the seizure attractor.

Grand mal seizure: Scalp EEG data

As with the Petit Mal seizure, we first investigate whether Grand Mal seizures correspond to the expression of nonlinear structure in scalp EEG. Figure 7 shows a seizure (Panel a) together with its nonlinear time series analysis (b). Prior to the seizure (t<80 s) there is evidence of nonlinear structure in the EEG only weakly at t~53 s. Immediately after the seizure onset (80-110 s) there exists evidence of nonlinearity in three of four consecutive epochs. There then follows a period (110-140 s) during which time, according to the nonlinear prediction technique, there is no evidence of nonlinear structure. Notably, the variance of the surrogate (null) distribution is particularly narrow during this period. The significance of this and the limitations of the nonlinear algorithm are discussed below. Strong nonlinear structure is then evident until the seizure terminates (~155 s). There is no nonlinearity evident for the remainder of the recording.

A corresponding model simulation is given in Panels (d-f): Nonlinear structure is evident weakly in the first half of the time series as v_{se} is held just below the bifurcation point (f). Strong nonlinear structure appears as soon as v_{se} crosses the bifurcation point and remains evident until the seizure offset. Subsequently, there is a period of time during which nonlinear structure is strongly suppressed. It weakly re-emerges once the alpha power is restored toward the end of the simulation (t>45 s).

Hence there is evidence for an increase in nonlinear structure in the Grand Mal data, although it much less striking than the Petit Mal seizure. Figure 7(c) shows the spectral density plot for the experimental data. As with the numerical seizure, increased power in the 10 Hz frequency peak coincides with the seizure onset (approx. 90 s). A peak persists throughout the seizure, although the peak frequency

slows considerably. At one stage (~100 s), two such peaks are visible. In comparison, the single peak frequency of the model seizure falls only marginally prior to the seizure offset (Fig. 6e). Of particular note is that, as with the model seizure, the experimental spectrum shows a marked post-ictal suppression of power across all frequencies (at ~155 s). As discussed above, this is the critical fingerprint of traversing the bistable 10 Hz bifurcation diagram. Such a feature is also reflected in the highly asymmetrical character of both the modeled and experimental seizure.

Another critical feature of the epilepsy spectrum is the extremely strong increase in broad spectrum (10-50 Hz) power from $t \sim 120$ s until seizure termination. Given that this is a scalp EEG recording, such power putatively reflects EMG contamination corresponding to the motor output of the seizure. It can be seen that this corresponds to the period of time during which the nonlinear prediction algorithm failed to find nonlinear structure in the data (Panel b). It is probable that any putative nonlinear structure would be obscured by the high amplitude noise, which also explains the small variance of the nonlinear index in the surrogate data. By comparison, no such EMG effect occurs in Petit Mal activity, so that the signal-noise ratio is more favorable.

The properties of the seizure are explored in further detail in Fig. 8. Panel (a) shows the onset of the seizure. A rapid nonlinear growth of orbit amplitude is clearly visible and this proves to be close to exponential. This is hence consistent with dynamical evolution away from an unstable spiral outset as observed in the model. Comparing the seizure onset with the seizure termination (b) reveals a number of features. Firstly, in distinction to the Petit Mal seizure, the waveform has changed markedly – suggesting nonstationarity of the dynamics. The frequency has fallen and the waveform now has spike and slow waves. Secondly, the abrupt seizure offset is visible, and thirdly, the post-ictal EEG suppression can be seen. The strong nonstationarity of the dynamics represents an additional obstacle for the nonlinear prediction algorithms employed in Fig. 7. However the marked temporal asymmetry of each oscillation visible just prior to seizure termination is a classic feature of nonlinear dynamics (Stam *et al.* 1998).

In the model seizure presented above, only the single parameter v_{se} was varied. It is inevitable that, during a lengthy seizure, other physiological parameters may vary as a consequence of the abnormally high activity and/or hypoxia resulting from disruptions to normal respiratory effort. Other parameters may additionally be varied by regulatory mechanisms in order to terminate the seizure (Engel *et al.* 1997, McCormick & Contreras 2001). One parameter that would be expected to vary is the

corticothalamic delay term t_0, as this depends upon axonal and synaptic transit times which may be hindered by both sustained high activity (Poolos *et al.* 1987) and hypoxia - leading, for example, to changes in ion concentration and diminished pre-synaptic neurotransmitter supply. The total transit time for a complete seizure also depends upon the membrane time constants α and β – which would also be affected by these factors (although we do not explicitly model these affects here).

A numerical simulation is presented in Fig. 9. This was obtained by increasing t_0 linearly from 80 ms to a "grossly pathological" 250 ms during the seizure, and then allowing it to return to its normal value after the seizure has terminated. The time series (a) and spectrum (b) reveal that the peak seizure frequency falls appreciably, as observed experimentally. The bistability "fingerprint" remains evident in the post-ictal spectral suppression. Introducing a second parameter nonstationarity has the additional effect of increasing the nonstationarity of the seizure waveform, so that a spike and slow wave morphology is now also observed in the model seizure (Panel c).

It must be emphasized that this is an exploratory illustration of varying one additional parameter after seizure initiation to simulate the secondary effect of a seizure (sustained high frequency neuronal activity in a hypoxic environment) on neuronal physiology. An attempt to capture all the variance in the seizure dynamics through manipulation of a large number of system parameters (within their pathophysiological ranges) will be the subject of future research.

Global Bifurcation Diagram

Figures 2(a) and 6(a) illustrate local bifurcation diagrams obtained by varying the single parameter v_{se}. Each can be thought of as a one dimensional cross-section through the larger 'global' bifurcation set spanned by all of the model's free parameters. It is natural to enquire as to the nature of such a set, which may shed light on a range of possible transitions to seizure activity in addition to being of mathematical interest in its own right.

The contrasting shape of the two local bifurcations suggests that they may be related through a simple 'unfolding' of the bistability region of Fig. 6(a) into the Hopf bifurcation of Fig 2(a). That is, the region of bistability would be expected to grow smaller until the fixed point became unstable to the left (rather than the right) of the onset of the large amplitude oscillations of Fig. 6(a). This hypothesis is motivated by the observation that such an unfolding is one of the basic geometric forms of all global bifurcation sets (Thom 1975). In order to test this hypothesis we generated a

series of bifurcation diagrams stretching between those of Figs 2(a) and 6(a) in parameter space. This was achieved by linear interpolation of all parameters that vary between these two figures, as given in columns 2 and 3 of Table 1. A total of 100 such intervening plots were produced. The pertinent plots are given in Fig. 10. In Panel (a) is the "tonic-clonic" bifurcation of Fig. 6 and in Panel (e) is the "Absence" bifurcation of Fig. 2. The critical transition between the two types of bifurcations occurs approximately 60-65% of the distance (in parameter space) between these two Panels. Panel (b) shows the interpolation at 61% of the distance. Surprisingly, it can be seen that the fixed point has undergone a Hopf type bifurcation *within* the zone of bistability. To the left of this instability, there hence exists both fixed point and high amplitude 10 Hz (aperiodic) oscillations: To right of this instability, the same 10 Hz oscillations coexist with smaller amplitude 3 Hz periodic oscillations. Panel (c) shows interpolation 63% of the distance. It can be seen that the Hopf bifurcation to 3 Hz activity occurs to the left of the region of bistability. Hence 10 Hz aperiodic and 3 Hz periodic oscillations coexist within this region. By 64% of the distance (Panel d), the Hopf and subsequent period-doubling bifurcations are now the only apparent nonlinear instabilities: The 10 Hz aperiodic branch of the tonic-clonic seizure cannot be accessed in this region of parameter space. Such a period doubling-type bifurcation set continues until the Absence case (Panel e) is reached.

Hence, rather than there being a smooth transition between the two bifurcations, we instead see that they intersect orthogonally. This implies that both seizure types may coexist in the same region of parameter space and reflects upon the complexity of the high dimensional dynamics of brain systems.

Conclusion

By performing the bifurcation analysis of a model of large-scale brain activity, this paper presents a parsimonious and unifying explanation of the defining features of the two major human generalized seizures – and their main differences. In summary, we observed a period-doubling bifurcation from healthy resting EEG to Absence (3Hz) seizures. This yielded time series realizations with periodic spike-and-wave morphology with close similarity to scalp EEG data taken from an Absence seizure data base. Moreover, the nature of the bifurcation set yields a symmetrical on-off character that is also found in the EEG data. In contrast, the bifurcation diagram for tonic-clonic (10Hz) seizures shows a sudden, discontinuous transition from damped (fixed point) dynamics to large-amplitude nonlinear oscillations with aperiodic behavior. The bifurcation set was of a "subcritical" nature – that is, associated with

bistable behavior. This yielded time series realizations compatible with tonic-clonic seizures. Critically, once the seizure commenced, the system displays high amplitude aperiodic oscillations and is required to traverse a considerable distance through parameter space before a stable (damped) linear regime re-emerges. This provides the explanation for the difference between pre- and post-ictal EEG spectra and cognitive states that is a defining feature of tonic-clonic seizures. This is the central finding of this study. It extends upon and tests the predictions concerning the onset of epileptic activity in Robinson *et al.* (2002) that seizure phenomena arises when corticothalamic dynamics lose linear stability in specific regions of parameter space. We are not aware of any prior unifying explanations for these key features of the generalized seizures.

A common criticism of many physiologically-based models of neural activity is that their numerous parameters undermine their explanatory power. Whilst this is an important consideration, a number of features of the current study are relevant in this regards. Firstly, the model we employed was not formulated specifically to generate seizure waveforms but rather to incorporate the critical features of corticothalamic dynamics to describe and predict the EEG temporal and spatial spectra in healthy resting and sleep states – when the activity is weakly damped and the nonlinearities can be neglected (Robinson *et al.* 1997, 2001, 2002, O'Connor *et al.* 2004). In the model, as in the clinical setting, seizures arise from 'background' resting EEG states when - due to a slight change in an underlying physiological property - the nonlinearity surpasses a critical threshold. The behavior of the model's dynamical variables during nonlinear dynamics permits predictions to be made regarding real physiological processes. In the present study, such prior predictions (Robinson *et al.* 2002) were further elaborated and compared to physiological data. Secondly, we observed that setting the model within the "resting state" regime but in the vicinity of a bifurcation point yielded weakly nonlinear alpha oscillations consistent with previous nonlinear analyses of resting EEG data (Stam *et al.* 1999, Breakspear & Terry 2002a). Thirdly, there are no free parameters in the sense that they all correspond to discrete physiological processes that have been constrained by independent empirical estimates and matched against a large data base of EEG spectra (Robinson *et al.* 2004). We used previously published parameters and did not perform any *a priori* exploration of parameter space. Fourthly, our numeric simulations yielded a number of phenomena which did lend themselves to potential refutation, such as the periodic nature of the Petit Mal seizures and the spectral properties of pre- and post ictal EEG. Finally, we employed a nonlinear prediction algorithm in order to test the main conjecture of the paper – that the onset of generalized seizures corresponds to a bifurcation from damped to strongly nonlinear behavior. The present

study hence represents a predictive application of an existing model in a novel direction, rather than an exploratory or confirmatory study.

Several interesting questions remain to be answered. Firstly, does the onset of the spike and slow wave morphology represent the smooth deformation of a limit cycle attractor, or the superposition of two cycles. The present study suggests the latter possibility, although this requires explicit analysis of the nonlinear stability properties of the limit cycle. Secondly, the corticothalamic model employed above does not explicitly include T-channels within the thalamus (although the present model is not inconsistent with such channels). T-channels, which show a refractory period following sustained bursting, have been incorporated into related neural population models of 3 Hz absence seizures (Destexhe & Sejnowski 2001). Destexhe and Sejnowski treated axonal propagation times as negligible and hence there was no time-delay. In comparison, the presence of time-delayed corticothalamic feedback is a crucial ingredient in the Petit Mal waveform we observed. In fact, qualitatively similar spike-wave oscillations can be generated by our model with a variety of time-delayed feedback loops which differ in some detail from those presented above. This is interesting, since it is known experimentally that Petit Mal seizures can arise as a result of changes in a number of different neuronal pathways. However, the present model incorporates the important components of the corticothalamic system together with the time delays that – due to finite axonal conduction speeds - are present in the brain (Meeren *et al.* 2002). Interestingly, although there are some differences in comparison to the Destexhe & Sejnowski model, both models emphasize the increased excitatory loops between the cortex and the specific and reticular nuclei of the thalamus underlying the generalized seizures. Thirdly, recent analysis reveals that spikes can be generated without any time-delayed loops at all: These may provide an explanation for purely cortically-generated spikes (McCormick & Contreras 2001).

For this study, we investigated a larger number of clinical seizures than were presented in the paper. However, the properties of these seizures that are pertinent to the validity of the model – such as the periodic waveform of the Petit Mal seizure – are the common and defining features of these seizure types and not at all limited to the examples presented. Furthermore, some features of the corticothalamic model seizures, such as the higher harmonics of the Grand Mal seizure (Figs 6e, 9b) were not present in our EEG examples. However, these harmonics are quite obvious in intra-cranial EEG recordings of Grand Mal seizures (Schiff *et al.* 2000), suggesting that they are simply obscured by the EMG activity present in scalp recordings.

It also important to note that the present paper employed primarily numerical analysis of the proposed corticothalamic model. Numerical analysis of delay-differential equations has its own caveats, such as the choice of the time-delayed values of the numerical interpolations. We chose a third-degree (cubic) interpolate and observed almost identical results for a variety of time. Increasing the time step or decreasing the accuracy of the time-delayed interpolates has the effect, as expected, of decreasing the values of v_{se} at which bifurcations occur. This is consistent with the presence of multiplicative numerical noise. We are currently undertaking a formal stability (Lyapunov) analysis in order to complement the results presented here.

To illustrate the effect of hypoxia and neural fatigue on the modeled Grand Mal seizure, we linearly increased the corticothalamic conduction delay. This had the effect of slowing the peak seizure frequency, imparting the "chirp" property observed in the clinical recordings (Schiff *et al.* 2000). Whilst it is unlikely that the corticothalamic delay would increase as markedly (from 80 ms to 250 ms) as in the exemplar seizure we present, it is probable that other physiological processes would also be affected by the impact of a grand mal seizure. Rather than attempting to study the influence of many changing parameters simultaneously, we choose to vary only a single likely target of hypoxia and neural fatigue – corticothalamic conduction time. Future work could study the manipulation of other model parameters. Such work, together with the incorporation of other physiological mechanisms into the model (such as T-channels) may have the effect of improving the match between the model seizure waveform and the properties of the clinical EEG. Mismatches between a model and the observed phenomena are, in fact, to be expected whenever relevant physiological mechanisms are omitted as they indicate precisely where the model is insufficient. Simply adding more and more detail to a model, however, without testing simpler realizations, adds to the validation problem discussed above. Critically, the present paper illustrates that a relatively simplified corticothalamic model is able to capture and explain the key features of the generalized seizures in a novel, unified manner. Physical models play an important integrative role in all of the physical sciences: There is no reason to believe that the brain should be an exception.

Acknowledgments

The authors would like to thank A. Bleasel for assisting with Absence data and R. Quian Quiroga for providing the tonic-clonic data. M.B. was a recipient of an American Psychiatric Association/AstraZeneca Research Award. JRT would like to acknowledge funding from the Nuffield Foundation via a newly appointed lecturer grant and the Leverhulme Trust for funding the Theoretical Neuroscience Network.

SR would like to acknowledge the financial support of the Loughborough University Sleep Research Centre and to the Bristol Laboratory for Applied Dynamical Engineering. The authors also acknowledge the support of an Australian Research Council grant and a University of Sydney SESQUI Research and Development grant.

References

Abraham, R.H., Shaw, C.D. (1992) *Dynamics – The Geometry of Behavior* Addison-Wesley: Redwood City.

Abramowitz, M., Stegun, I.A. (1970) *Handbook of Mathematical Functions.* Dover Publications: New York.

Andrezejak, RG, Laehnertz, K, Mormann, F, Rieke, C, David, P, Elger, CE (2001) Indications of nonlinear deterministic and finite-dimensional structure in time series of brain electrical activity: Dependence on recording region and brain state. *Phys. Rev. E* **64**: 061907.

Arnhold J, Grassberger P, Lehnertz K, Elger C (1999) A robust method for detecting interdependencies: application to intracranially recorded EEG. *Physica D,* **134**:419-430.

Breakspear, M. (2002) Nonlinear phase desynchronization in human electroencephalographic data. *Human Brain Mapping* **15**: 175-198 .

Breakspear, M, Terry, J (2002) Detection and description of nonlinear interdependence in normal multichannel human EEG. *Clinical Neurophysiology* **113**: 735-753.

Breakspear, M., Terry, J., Friston, K. (2003) Modulation of excitatory synaptic coupling facilitates synchronization and complex dynamics in a nonlinear model of neuronal dynamics. *Network: Computation in Neural Systems* **14:** 703–732

Breakspear, M., Williams, L., Stam, K. (2004) Topographic analysis of phase dynamics in neural systems reveals formation and dissolution of 'dynamic cell assemblies'. *Journal of Computational Neuroscience* **16**: 49-68.

Breakspear, M. (2004) "Dynamic" connectivity in neural systems: Theoretical and empirical considerations. *Neuroinformatics*, **4**:1-23.

Casdagli M (1989) Nonlinear prediction of chaotic time series. *Physica D,* **35**:335-357.

Crevier, DW, Meister, M (1998) Synchronous period-doubling in flicker vision of salamander and man. *J. Neurophysiol.* **79**: 1869-1878.

Daffertshofer, A., Peper,C.E., Frank, T.D., Beek, P.J. (2000) Spectral analysis of event-related encephalographic signals. *Hum Mov Sci* **19**: 475-498.

Dammig M, Mitschke F (1993) Estimation of Lyapunov exponents from time series: the stochastic case. *Physics Letters A*, **178**:385-394.

Destexhe, A., Sejnowski, T.J. (2001) *Thalamocortical Assemblies.* Oxford University Press: Oxford.

Engel, J., Dichter, M.A., Schwartzkroin, P.A. (1997) Basic mechanisms of human epilepsy, In: *Epilepsy: A Comprehensive Textbook* (ed. Engel, J., Pedley, T.A.) Lippincott-Raven: Philadelphia.

Feucht, M, Moller, U, Witte, H, Schmidt, K, Arnold, M, Benninger, F, Steinberger,K, Friedrich, MH (1998) Nonlinear dynamics of 3Hz Spike-and-wave discharges recorded during typical absence seizures in children. *Cerebral Cortex,* **8**: 524-533.

Freeman W (1975) *Mass Action in the Nervous System: Examination of the Neurophysiological Basis of Adaptive Behaviour through the EEG,* Academic Press: New York.

Freeman WJ, Rogers LJ, (2002) Fine temporal resolution of analytic phase reveals episodic synchronization by state transitions in gamma EEGs. *J Neurophysiol* **87**: 937-945.

Friston, KJ, Jezzard, PJ, Turner, R (1994) Analysis of functional MRI time-series. *Human Brain Mapping* **1**: 153-171.

Friston, KJ (2000) The labile brain. I. Neuronal transients and nonlinear coupling. *Philosophical Transactions of the Royal Society of London*, **355B:** 215-236.

Fuchs, A., Mayville, J.M., Cheyne, D., Weinberg, H., Deecke, L., Kelso, J.A.S. (2000) Spatiotemporal analysis of neuromagnetic events underlying the emeregence of coordinative instabilities. *NeuroImage* **12**: 71-84.

Gratton, G., Coles, M., and Donchin, E. 1983. A new method for off-line removal of ocular artifact. *Electroencephalogr. Clin. Neurophysiol.* **55**: 468-484.

Izhikevich, E (2001) Synchronization of elliptic bursters. *SIAM Review* **43**: 315-344.

Jirsa, VK, Haken, H (1996) Field theory of electromagnetic brain activity. *Physical Review Letters*, **77**: 960-963.

Kelso J, Bressler S, Buchanan S, DeGuzman G, Ding M, Fuchs A, Holroyd T (1992), A phase transition in human brain and behaviour. *Physics Letters A*, **169**: 134-144.

Lopes da Silva F, Blanes W, Kalitzin SN, Parra J, Suffczynski P, Velis DN. (2003) Epilepsies as dynamical diseases of brain systems: Basic models of the transition between normal and epileptic activity. *Epilepsia.* **44**:72-83.

McCormick, D.A., Contreras, D. (2001) On the cellular and network bases of epileptic seizures. *Annu. Rev. Physiol.*, **63**: 815-846.

Meeren, H.K., Pijn, J.P., Van Luijtelaar, E.L., Coenen, A.M., Lopes da Silva, F.H. (2002), Cortical focus drives widespread corticothalamic networks during spontaneous absence seizures in rats. *J. Neurosci.* **22**: 1480-1495.

Nunez, PL (1974), The brain wave equation: a model for the EEG. *Mathematical Biosciences*, **21**: 279-297.

Nunez, PL (1995) *Neocortical Dynamics and Human EEG Rhythms*, Oxford University Press: Oxford.

O'Connor, SC, Robinson, PA, Chiang, AKI (2002) Wavenumber spectra of EEG signals. *Phys. Rev. E*, **66**: 061905.

Perez Valezquez, J.L., Cortez, M.A., Carter Snead III, O., Wennberg, R. (2003) Dynamical regimes underlying epileptiform events: role of instabilities and bifurcations in brain activity. *Physica D* **186**: 205-220.

Poolos, N.P., Mauk, M.D., Kocsis, J.D. (1987) Activity-evoked increases in extracellular potassium modulates presynaptic excitability in the CA1 region of the hippocampus. *J. Neurophysiol.* , **58**: 404-416.

Prichard D, Theiler J (1994) Generating surrogate data for time series with several simultaneously measured variables. *Phys. Rev. Lett.*, **73**:951-954.

Quian Quiroga, R., Garcia, H., Rabinowich, A. (2002) Frequency evolution during tonic-clonic seizures. *EMG Clin. Neurophysiol.* **42**: 323-331.

Robinson, PA, Rennie, CJ, Wright, JJ (1997) Propagation and stability of waves of electrical activity in the cerebral cortex. *Phys. Rev. E,* **56**: 826-840.

Robinson, PA, Rennie, CJ, Wright, JJ, Bahramali, H, Gordon, E, Rowe, DL (2001) Prediction of electroencephalographic spectra from neurophysiology. *Phys. Rev. E,* **63**: 021903.

Robinson, PA, Rennie, CJ, Rowe, DL (2002) Dynamics of large-scale brain activity in normal arousal states and epileptic seizures. *Phys. Rev. E,* **65**: 041924.

Robinson, PA, Rennie, CJ, Rowe, DL, O'Connor, SC (2004) Estimation of multiscale neurophysiologic parameters by electroencephalographic means. *Human Brain Mapping* **23**: 53-72.

Rombouts S, Keunen R, Stam C (1995) Investigation of nonlinear structure in multichannel EEG. *Physics Letters A,* **202**:352-358.

Schiff, S, So, P, Chang, T, Burke, R, Sauer, T (1997) Detecting dynamical interdependence and generalized synchrony through mutual prediction in a neural ensemble. *Physical Review E,* **54**: 6708-6724.

Schiff, S, Colella, D, Jacynac, GM, Hughes, Creekmore, JW, Marshall, A, Bozek-Kuzmicki, M, Benkec, G, Gaillard, WD, Conry, J, Weinstein, SR (2000) Brain Chirps: Spectrographic signatures of epileptic seizures. *Clin. Neurophysiol.,* **111**: 953-958.

Stam CJ, Pritchard W (1997a) Dynamics underlying rhythmic and non-rhythmic variants of abnormal, waking delta activity. *Int. J. Psychophysiol.*, **34**: 5-20.

Stam CJ, van Woerkom T, Keunen R (1997b) Nonlinear analysis of the EEG in Creutzfeldt-Jakob disease. *Biological Cybernetics*, **77**:247-256.

Stam CJ, Pijn J, Pritchard W (1998) Reliable detection of nonlinearity in experimental time series with strong periodic components. *Physica D,* **112**:361-380.

Stam CJ, Pijn J, Suffczynski P, Lopes da Silva (1999) Dynamics of the alpha rhythm: evidence for non-linearity? *Clinical Neurophysiology,* **110**:1801-1813.

Stam, CJ, van Dijk, BW (2002) Synchronization likelihood: An unbiased estimate of generalized synchronization in multivariate data sets *Physica D,* **163**: 236-251.

Terry, J., Breakspear, M. (2003) An improved algorithm for the detection of nonlinear interdependencies *Biological Cybernetics* **88**: 129-136.

Theiler J, Eubank S, Longtin A, Galdrikian B, Farmer, J (1992) Testing for nonlinearity: the method of surrogate data. *Physica D*, **58**: 77-94.

Thom, R. (1975) *Structural Stability and Morphogensis*. W.A. Benjamin: Reading, MA.

Wendler, F, Bartolomei, F., Bellanger, JJ, Chauvel, P (2002) Epileptic fast activity can be explained by a model of impaired GABAergic dendritic inhibition *Eur. J. Neurosci.* **15**: 1499-1508.

Wright JJ, Kydd R, Lees G (1985) State changes in the brain viewed as linear steady-states and nonlinear transitions between steady-states. *Biological Cybernetics,* **53**:11-17.

Zifkin, B., Dravet, C. (1997) Generalized convulsive seizure, In: *Epilepsy: A Comprehensive Textbook* (ed. Engel, J., Pedley, T.A.) Lippincott-Raven: Philadelphia.

Appendix A

In this appendix we first give the eight first order delay-differential equations describing the brain in the spatially uniform case, followed by an outline of the stability variables *x*, *y*, and *z*.

A1. First order delay-differential equations for the spatially uniform model

We assume that intracortical connectivities are proportional to the numbers of synapses involved, implying $V_i=V_e$ and $Q_i=Q_e$ (Robinson *et al.* 2002), so that the cortical inhibitory and excitatory processes are enslaved. The smallness of r_i and the thalamic nuclei allow us to set $\gamma_c \approx \infty$, $c=i,r,s$, yielding the local approximation from Eqs. (2) and (7), $\phi_c(t)=S[V_c(t)]$.

Thus from Equations (2) and (4-7), we obtain

$$\frac{d\phi_e(t)}{dt} = \dot{\phi}_e(t) \tag{A1}$$

$$\frac{d\dot{\phi}_e(t)}{dt} = \gamma_e^2 (S(V_e(t)) - \phi_e(t)) - 2\gamma_e \dot{\phi}_e(t) \tag{A2}$$

$$\frac{dV_e(t)}{dt} = \dot{V}_e(t) \tag{A3}$$

$$\frac{d\dot{V}_e(t)}{dt} = \alpha\beta(\nu_{ee}\phi_e(t) + \nu_{ei}S(V_e(t)) + \nu_{es}S(V_s(t-t_0/2)) - V_e(t)) - (\alpha+\beta)\dot{V}_e(t) \tag{A4}$$

$$\frac{dV_s(t)}{dt} = \dot{V}_s(t) \tag{A5}$$

$$\frac{d\dot{V}_s(t)}{dt} = \alpha\beta(\nu_{se}\phi_e(t-t_0/2) + \nu_{sr}S(V_r(t)) + \nu_{sn}\phi_n(t) - V_s(t)) - (\alpha+\beta)\dot{V}_s(t) \tag{A6}$$

$$\frac{dV_r(t)}{dt} = \dot{V}_r(t) \tag{A7}$$

$$\frac{d\dot{V}_r(t)}{dt} = \alpha\beta(\nu_{re}\phi_e(t-t_0/2) + \nu_{rs}S(V_s(t)) - V_r(t)) - (\alpha+\beta)\dot{V}_r(t) \tag{A8}$$

A2. Reduced parameter space

Linear stability analysis suggests a three-dimensional parameterization of low frequency instabilities, defining an *xyz* coordinate space by (Robinson *et al.* 2002)

$$x = G_{ee}/(1-G_{ei}), \tag{A9}$$

$$y = \frac{G_{ese}+G_{esre}}{(1-G_{srs})(1-G_{ei})}, \tag{A10}$$

$$z = -G_{srs}\alpha\beta/(\alpha+\beta)^2, \tag{A11}$$

where gain $G_{ab}=\rho_a v_{ab}$ is the response in neurons a to unit input from neurons b, sigmoid slope $\rho_a=dS(V_a)/dV_a$, with $G_{ese}=G_{es}G_{se}$, $G_{esre}=G_{es}G_{sr}G_{re}$, and $G_{srs}=G_{sr}G_{rs}$ for convenience. In previous work, these parameters have only been used in the steady state where they were derived. Here we take them to define a coordinate transformation of the dynamical variables V_a.

Figure captions

Figure 1

Linear stability zone for the corticothalamic model within the truncated space spanned by the three stability variables *x*, *y*, and *z*. The shaded surface represents the values at which the system loses instability at slow (red), spindle (blue) and alpha frequencies (green). Within the tent are shown representative values for eyes closed, eyes open and sleep stages 1, 2, and 4. The present study concerns the onset of nonlinear oscillations as the system passes outside of the stability zone.

Figure 2

Results for 3 Hz bifurcation analysis in the corticothalamic model. (a) Bifurcation diagram. Time series of (b) the cortical excitatory field potentials ϕ_e and (c) the corresponding (noise perturbed) corticothalamic 'gain parameter v_{se}. Period doubling oscillations evident at the seizure onset (d) and offset (e). (f) Color contour representation of the dynamic spectrogram of ϕ_e. (g) Time delayed phase portrait of the seizure onset transient and seizure attractor. Arrows indicate the direction of flow. (h) Seizure plotted within the phase space spanned by the "stability parameters" *x*, *y*, and *z*. (i) Dynamics of the cortical ϕ_e (solid) specific thalamic ϕ_s (dotted) and reticular thalamic ϕ_r (dashed) activities.

Figure 3

Nonlinear time series analysis of the EEG Petit Mal seizure (left column) and corticothalamic 3Hz seizure (right column). (a) EEG seizure (F_3 electrode) and (b) evolution of the "nonlinear predictability index" (NPI). Solid line is the real data and dotted lines are derived from the 19 surrogate data sets. (c) Excitatory cortical field potential ϕ_e and (d) corresponding NPI evolution of the corticothalamic model. Arrows show instances of "weak" nonlinear structure (slight increases in the real compared to the surrogate nonlinear indices) before and after the seizure.

Figure 4

Analysis of scalp EEG data from channel F_z. (a) Entire seizure and (b) corresponding dynamic spectrogram showing strong 3 Hz peak and multiple harmonics. Seizure (c) onset and (d) offset. (e) Time-delayed phase portrait. (f) Peak-to-peak frequency first return map.

Figure 5

Nonlinear and linear characteristics of scalp EEG (a-d) and modeled cortical field potentials (e-h). (a) A pair of posterior bipolar EEG recordings which exhibit nonlinear interdependence. (b) The same electrodes where there was only linear interdependence. (c) Spectra of panel a. (solid) and b. (dashed), (d) Nonlinear prediction errors for 20 future iterates. Dashed lines are for surrogate data. The plain solid line shows the lower limit of the null (surrogate) realizations (from Breakspear & Terry 2002). The two solid lines with crosses show the results for the bipolar recordings in (a) and (b). The lower of these is from panel (a). Time series realizations of the model with (e) v_{se}=10.4x10^{-4} and (f) v_{se}=10.1x10^{-4}. (g) Power spectra of panel e. (solid) and f. (dashed). (h) The solid lines with crosses are the nonlinear prediction errors for panel (e) and (f). The lower of these is from panel (e).

Figure 6

Bifurcation diagram for the 10Hz instability for (a) ϕ_e and (b) V_e. Both are plotted left to right in black and thence right to left in red. The bistable window is evident when both black and red are visible (otherwise the black is overlaid by red). Arrows in panel (a) mark the sequence of events described in the text. Numerical time series for ϕ_e (c) with corresponding values of the state parameter v_{se}. Arrows are as for panel (a). (e) Corresponding dynamic spectrogram. (f) Close-up of seizure onset, showing exponential growth of amplitudes. (g) Phase portrait spanned by the three field potentials ϕ_e, ϕ_s, and ϕ_r. Red shows transient outset from the (unstable) fixed point. Black shows aperiodic attractor.

Figure 7

Nonlinear time series analysis of the EEG Grand Mal seizure (left column) and corticothalamic 10 Hz seizure (right column). (a) EEG seizure (C_z electrode) and (b) evolution of the "nonlinear predictability index" (NPI). Solid line is the real data and dotted lines are derived from the 19 surrogate data sets. (c) Corresponding spectra of seizure. (d) Excitatory cortical field potential ϕ_e, (e) corresponding NPI evolution of corticothalamic model and the corresponding (noise perturbed) corticothalamic parameter v_{se} (f).

Figure 8

Close-up image of (a) the onset and (b) offset of the EEG Grand Mal seizure depicted in Figure 6. Note the nonlinear amplitude growth during the seizure onset.

Figure 9

Numerical simulation of the corticothalamic model with additional linear increase of corticothalamic delay time t_0 during the seizure. (a) Entire seizure. (b) Spectrum. (c) Close-up of the seizure termination.

Figure 10

Global bifurcation diagram, visdualised by linear interpolation of all parameters between those for the (a) 10 Hz instability and (e) 3 Hz instability. Interpolates at (b) 61%, (c) 63% and (d) 64% of the interpolated distance, in parameter space, between (a) and (e).

Figure 1

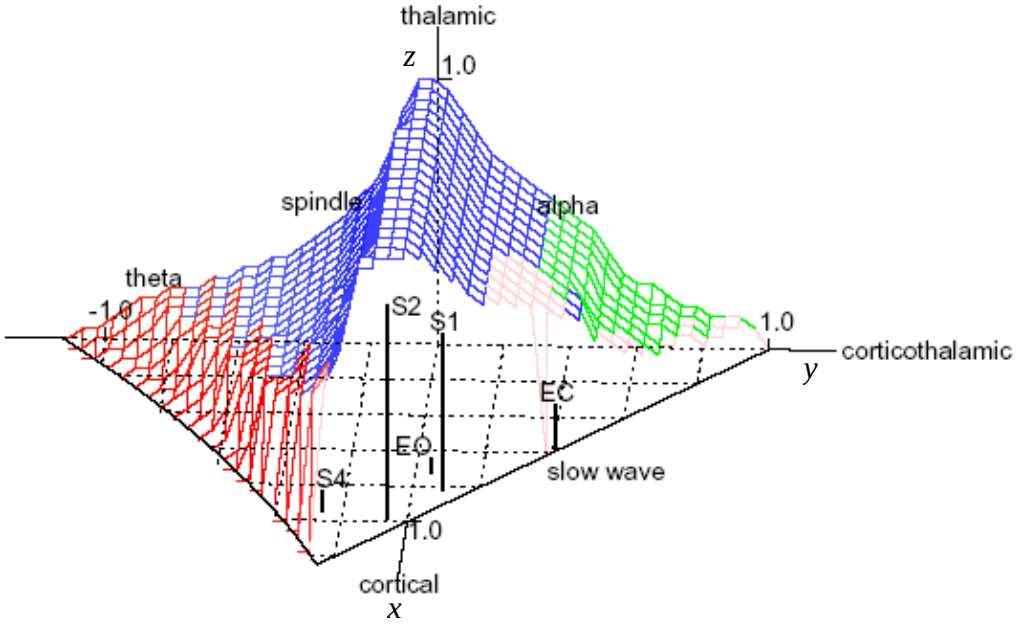

Breakspear, *et al.* (2005)

Figure 1

Figure 2

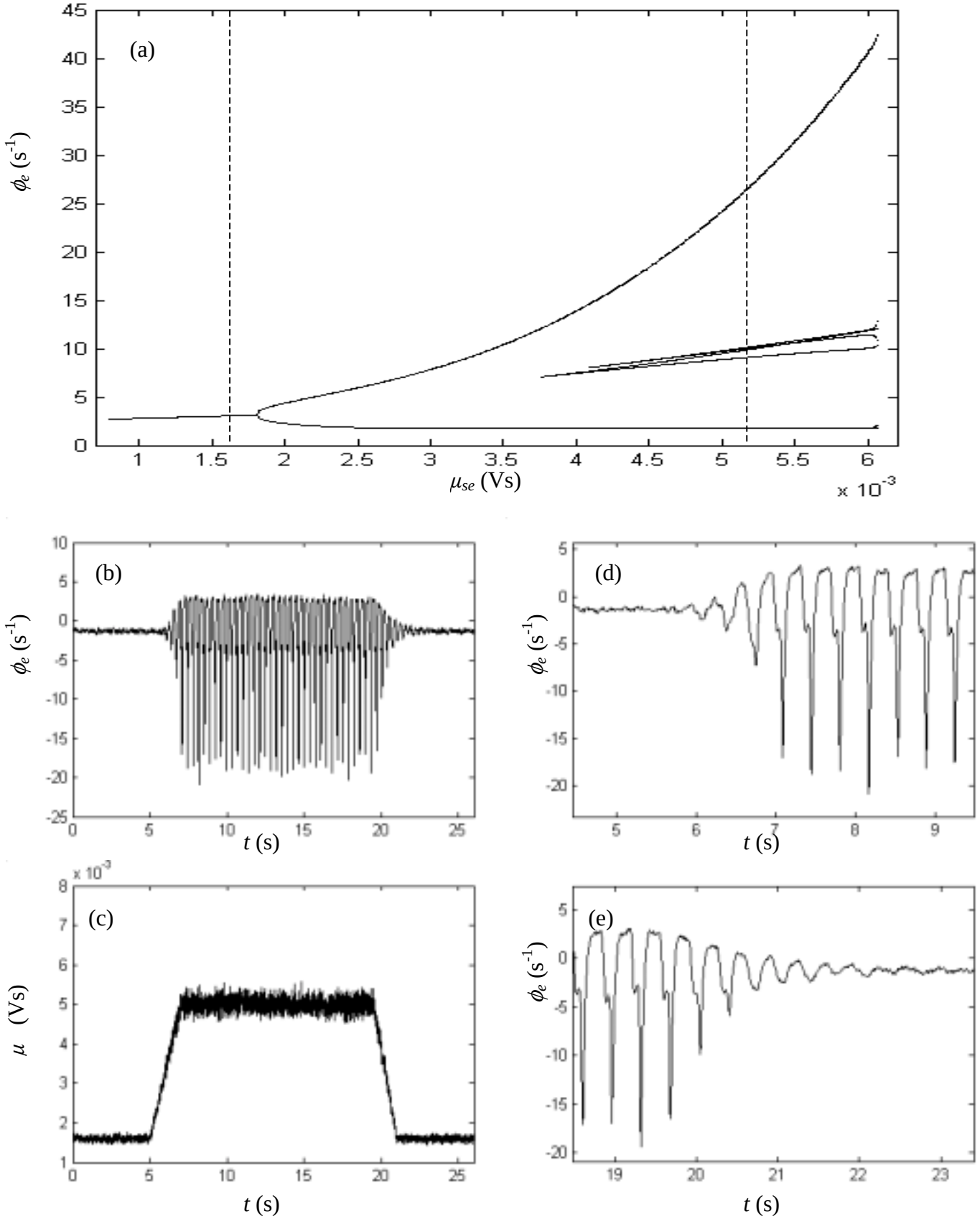
(a)
ϕ_e (s^{-1})
μ_{se} (Vs)
x 10^{-3}
(b)
ϕ_e (s^{-1})
t (s)
(d)
ϕ_e (s^{-1})
t (s)
(c)
x 10^{-3}
μ (Vs)
t (s)
(e)
ϕ_e (s^{-1})
t (s)

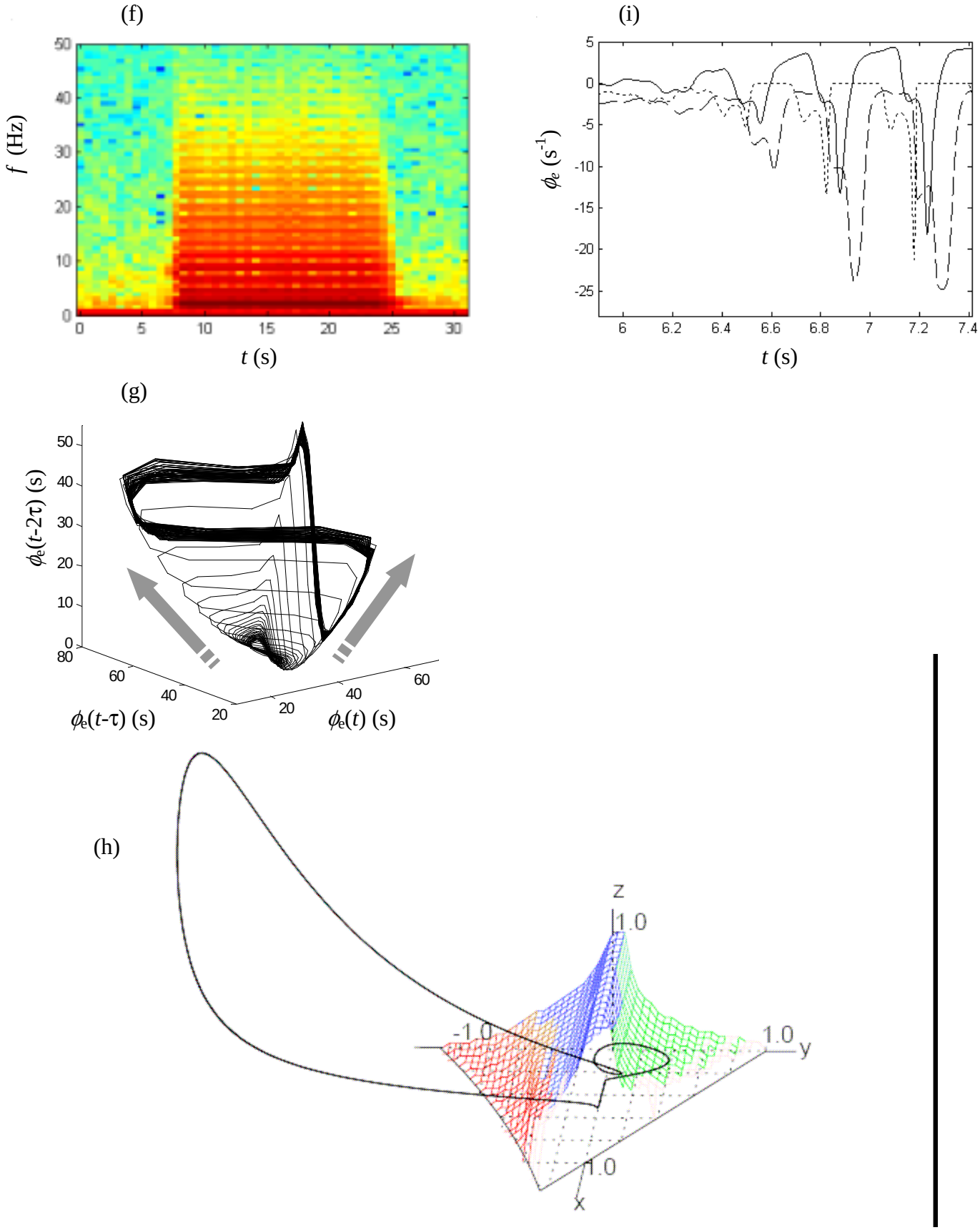

Breakspear, *et al.* (2005)

Figure 2

Figure 3

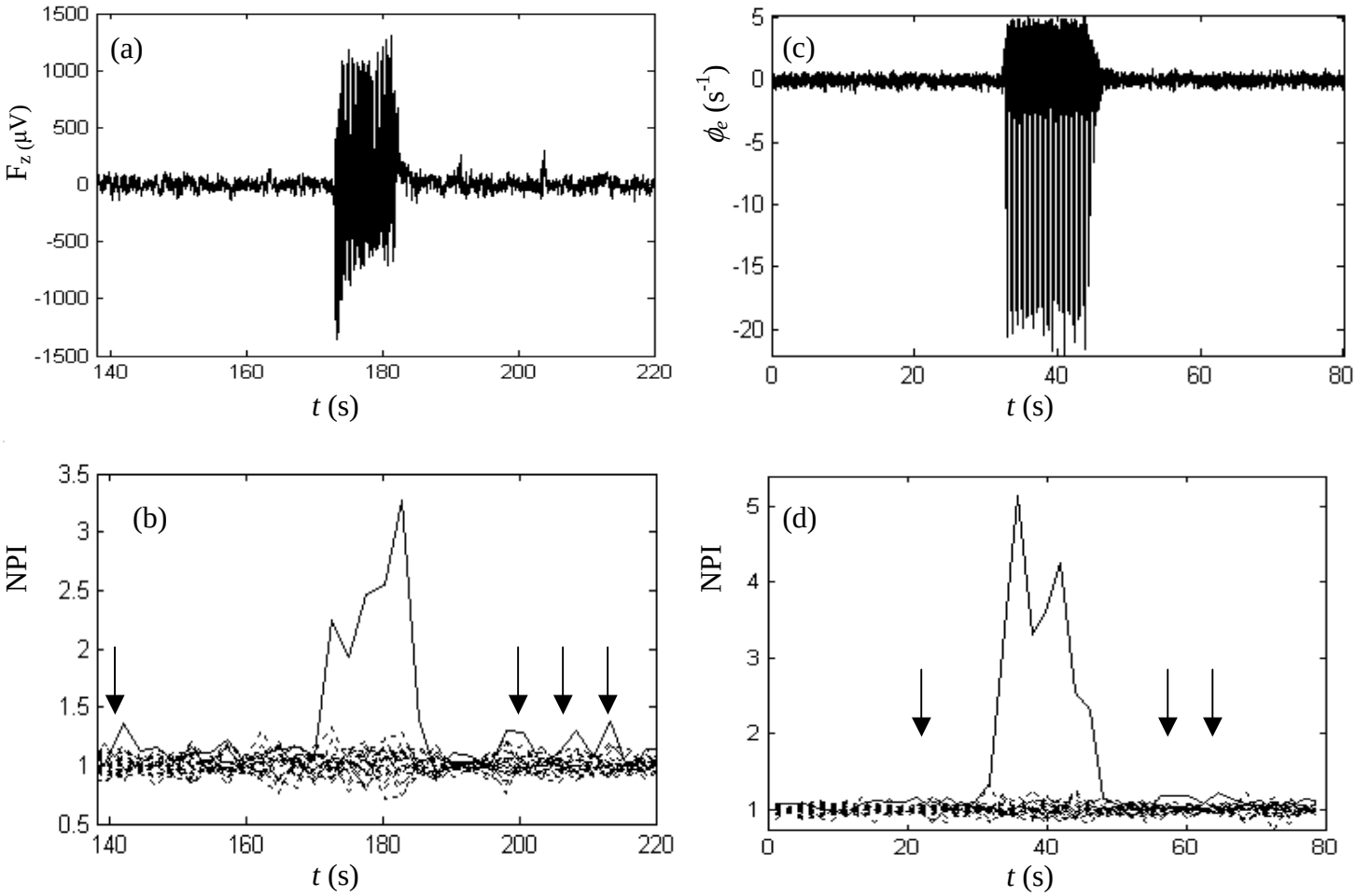

Breakspear, *et al.* (2005)

Figure 3

Figure 4

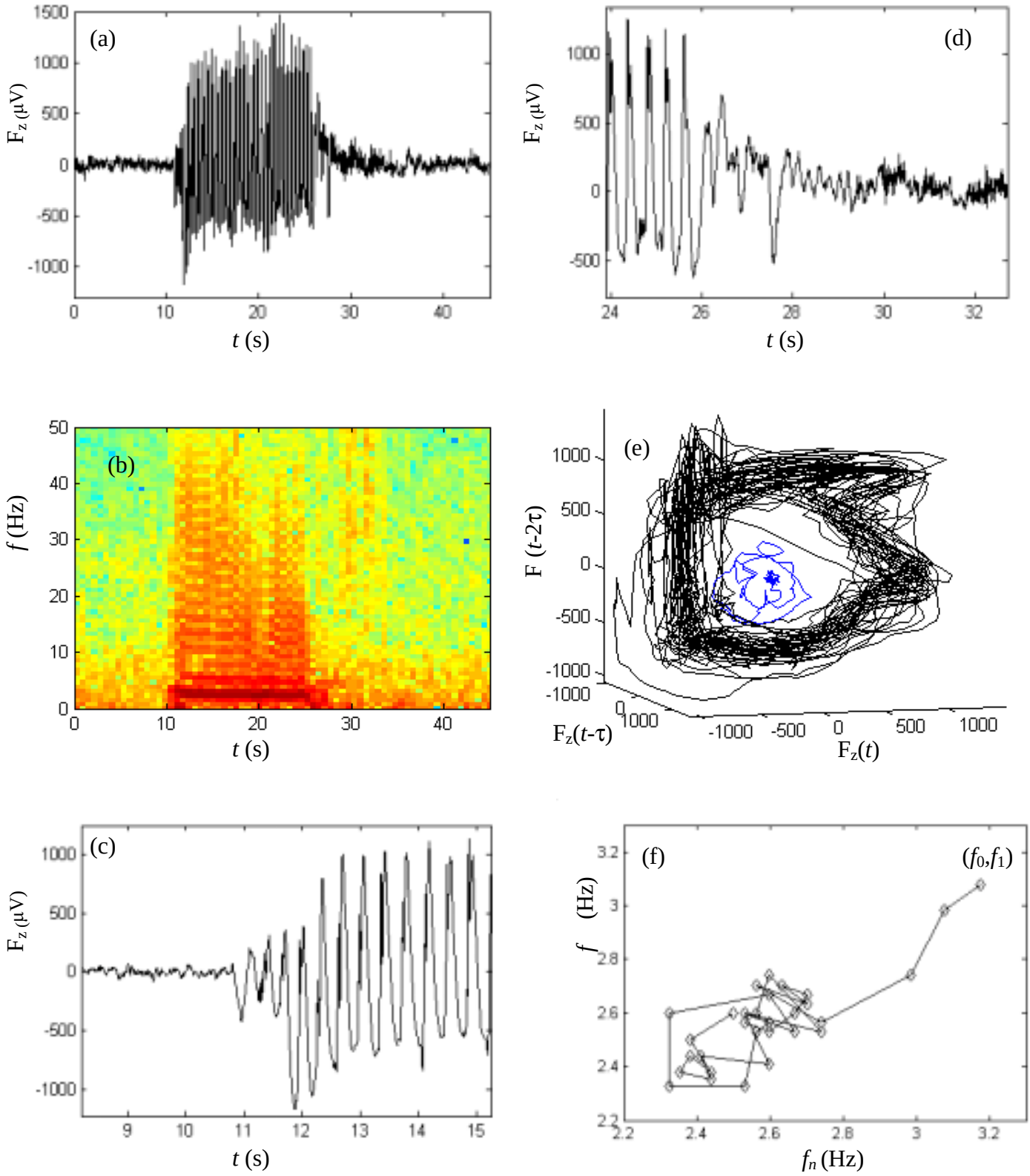

Breakspear, *et al.* (2005)

Figure 4

Figure 5 (a)-(d)

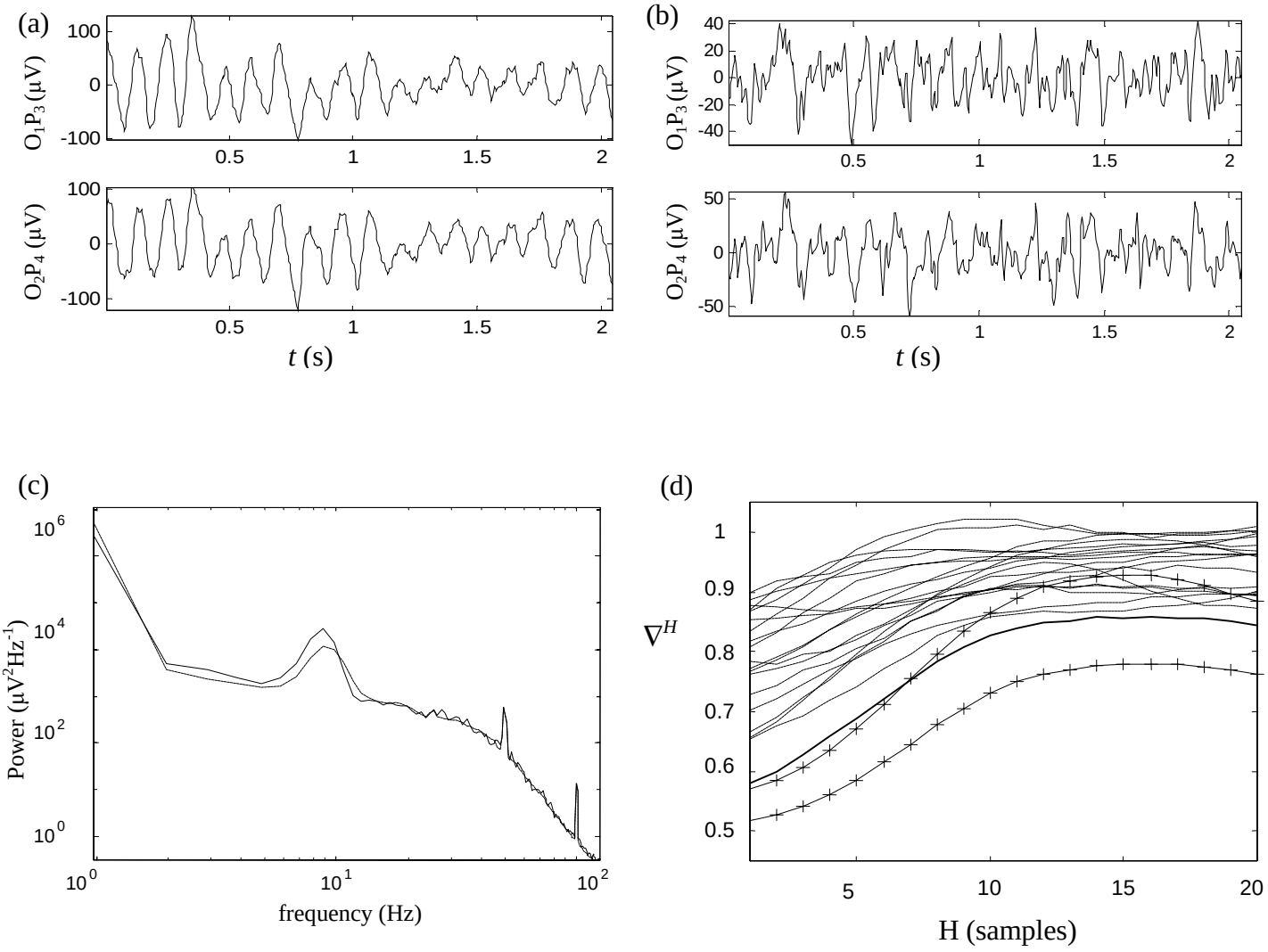

Breakspear, *et al.* (2005)

Figure 5 (a) – (d)

Figure 5 (e)-(h)

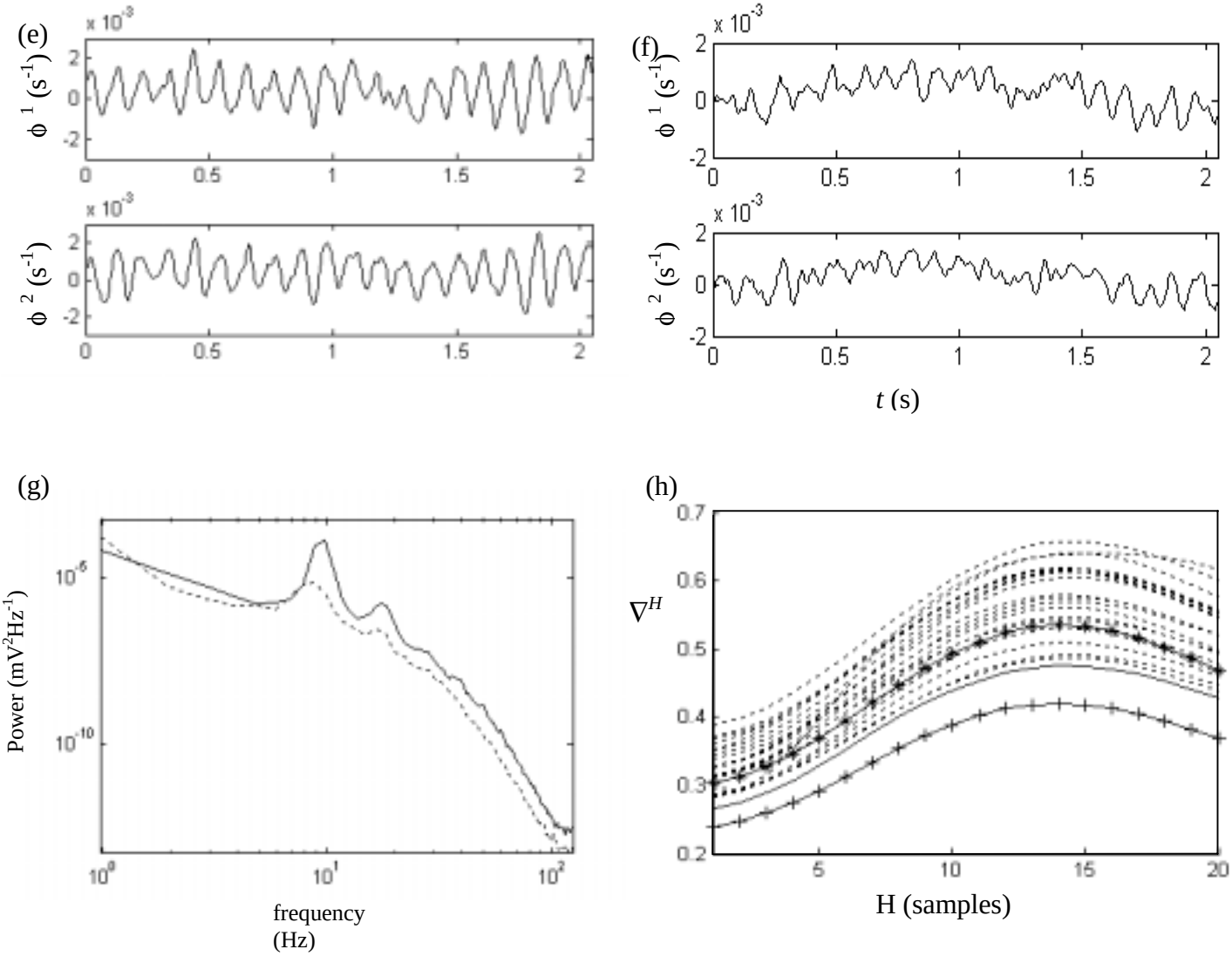

Breakspear, *et al.* (2005)

Figure 5 (e) – (h)

Figure 6

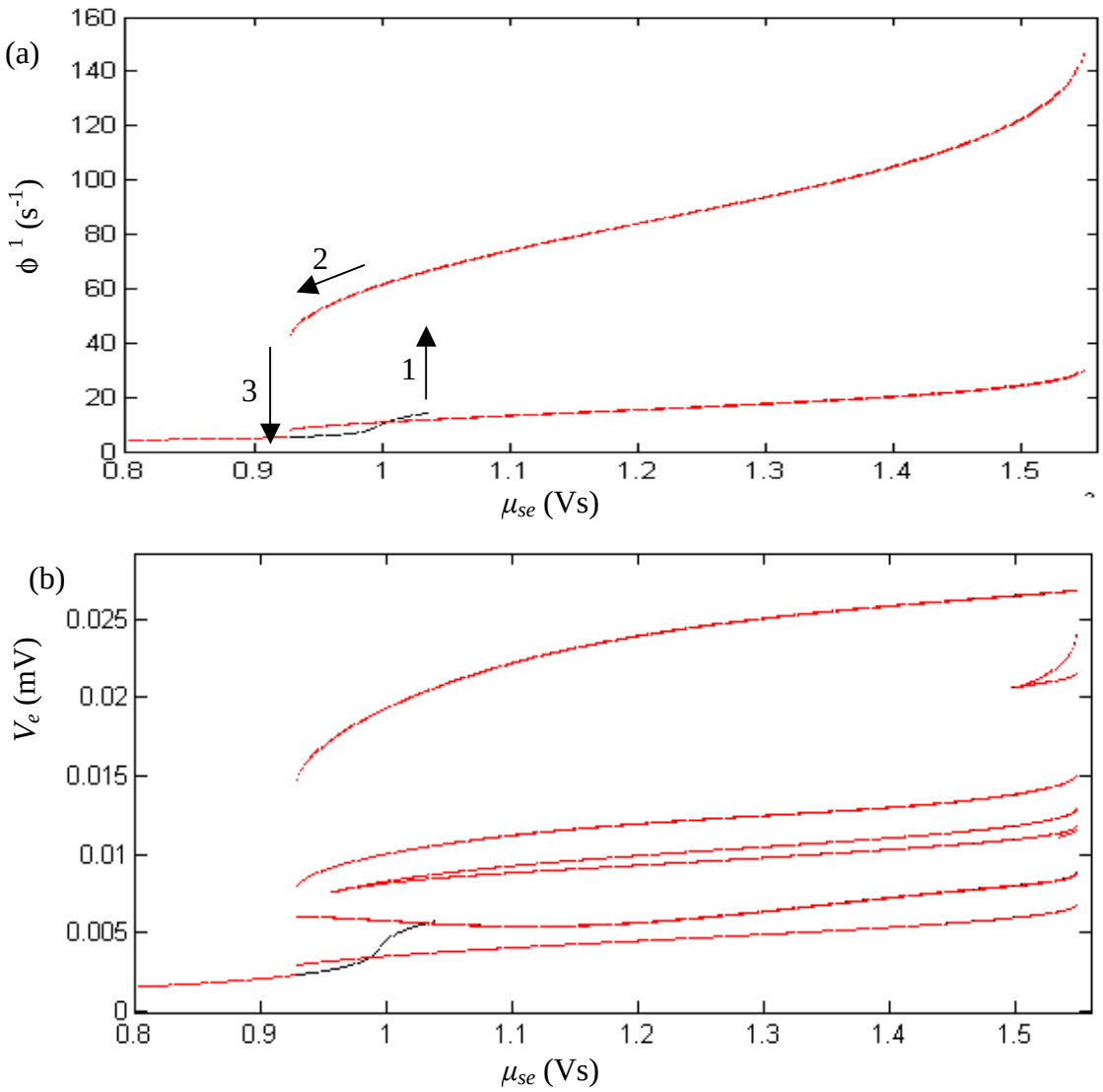

Breakspear, *et al.* (2005)

Figure 6(a)-(b)

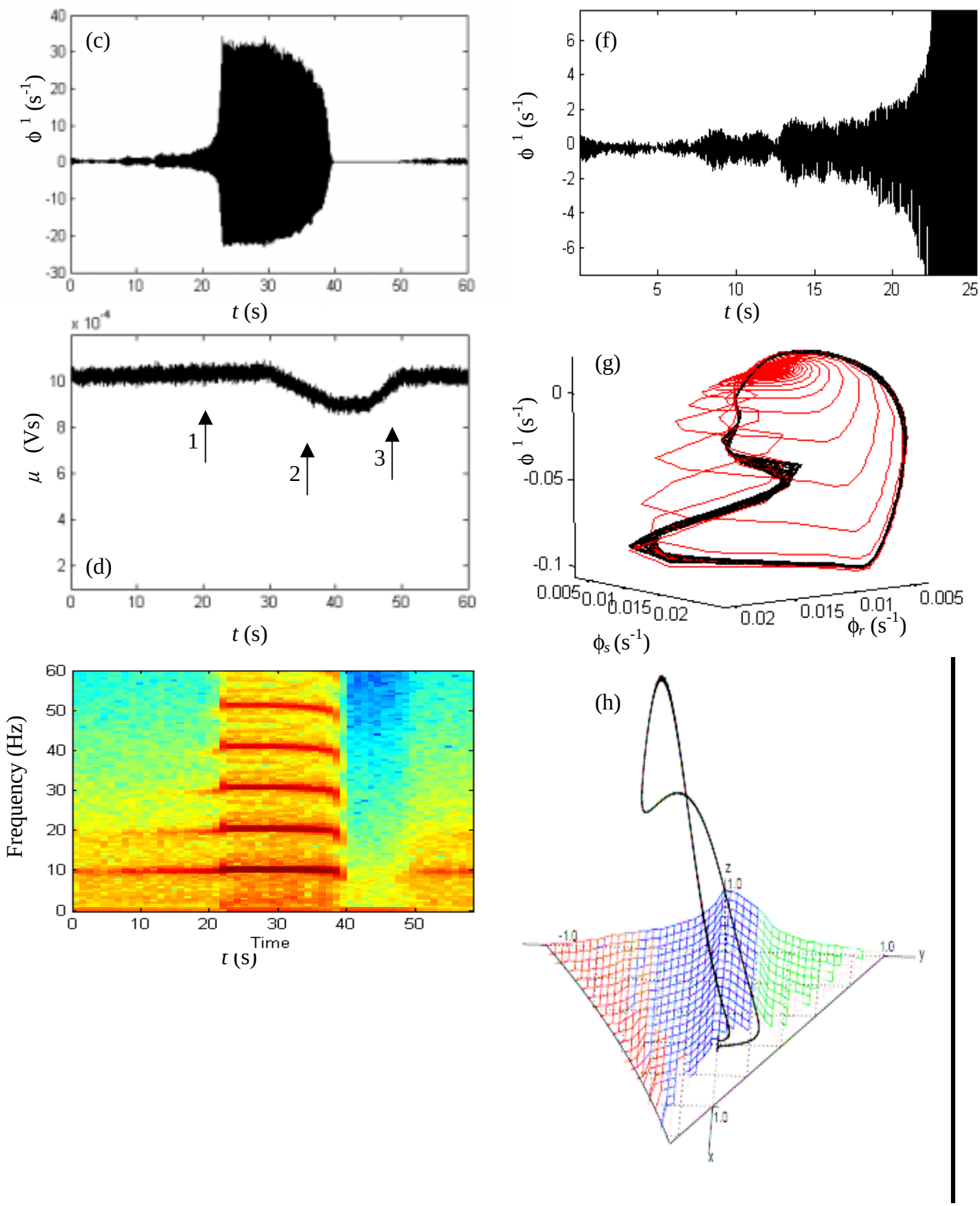

Breakspear, *et al.* (2005)

Figure 6 (c)-(h)

Figure 7

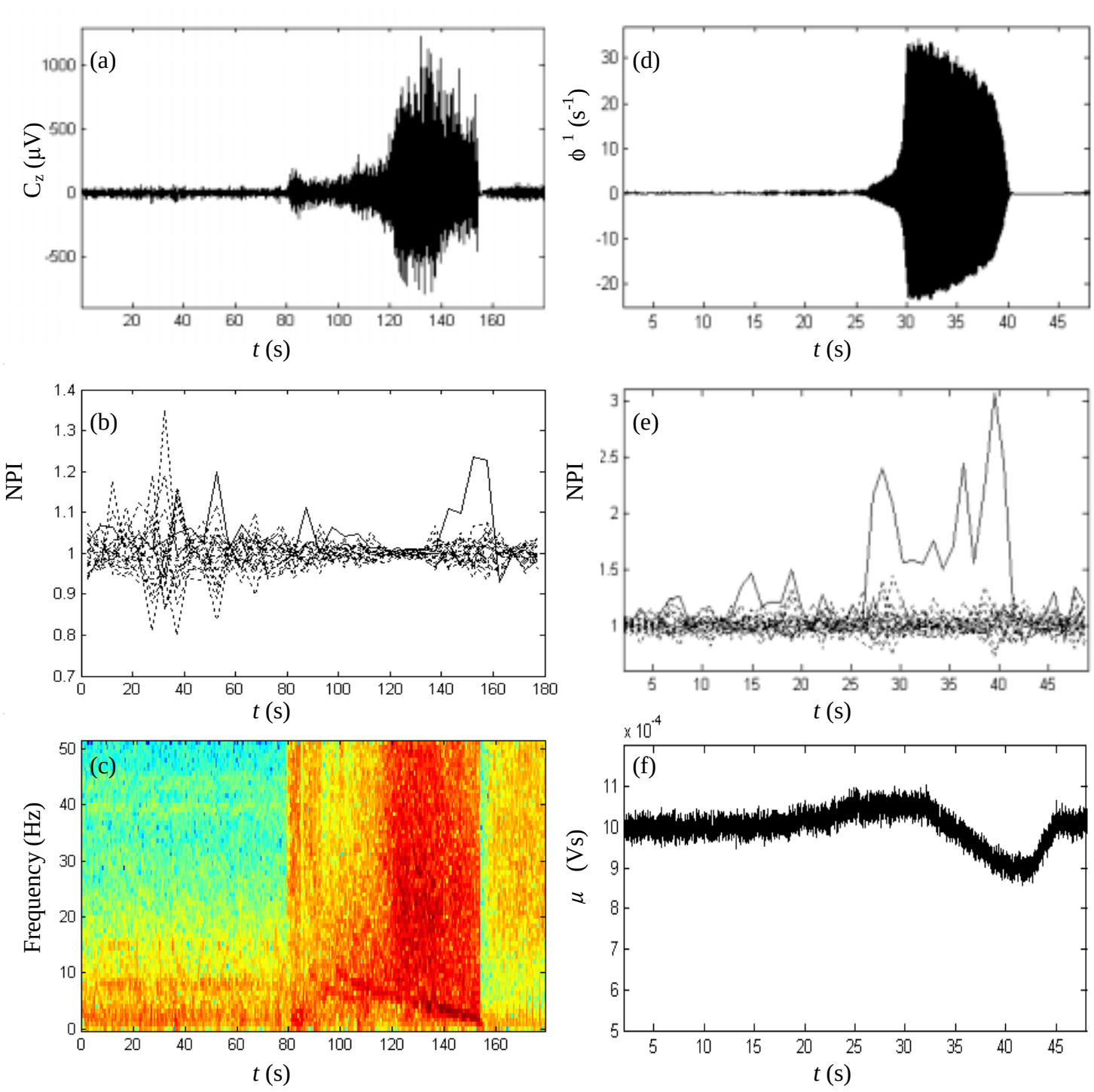

Breakspear, *et al.* (2005)

Figure 7

Figure 8

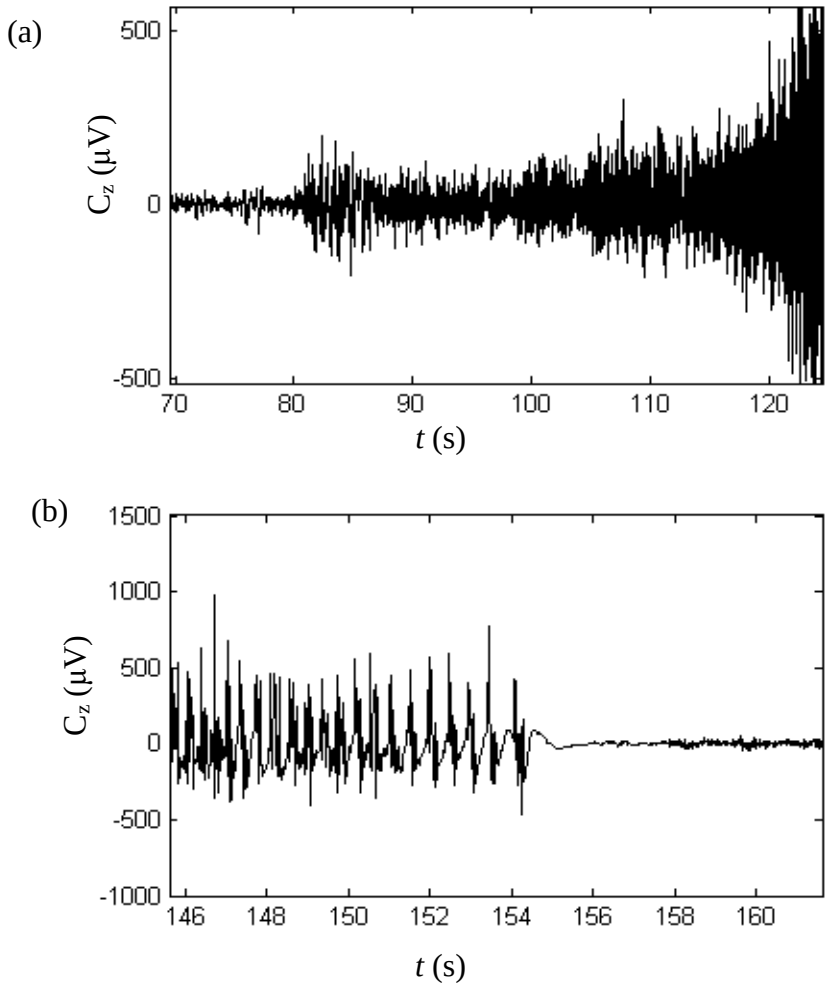

Breakspear, *et al.* (2005)

Figure 8

Figure 9

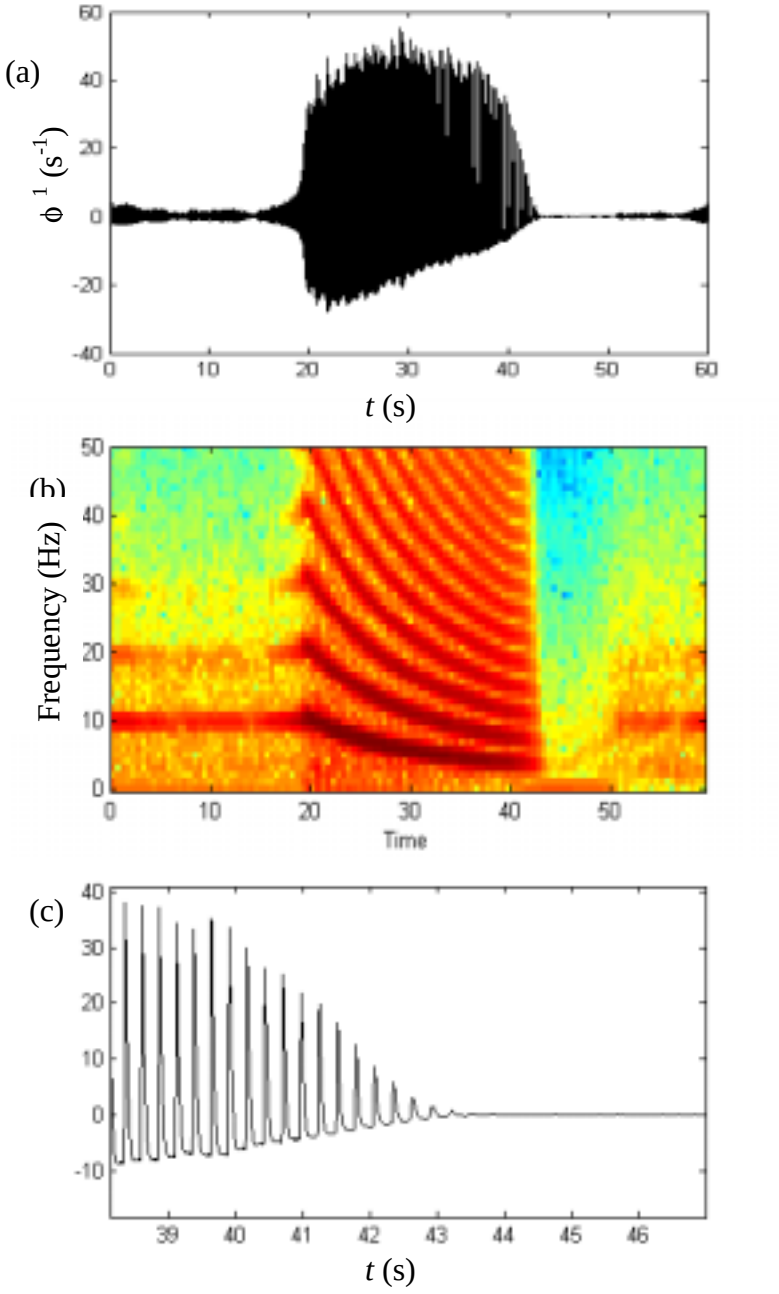

Breakspear, *et al.* (2005)

Figure 9

Figure 10

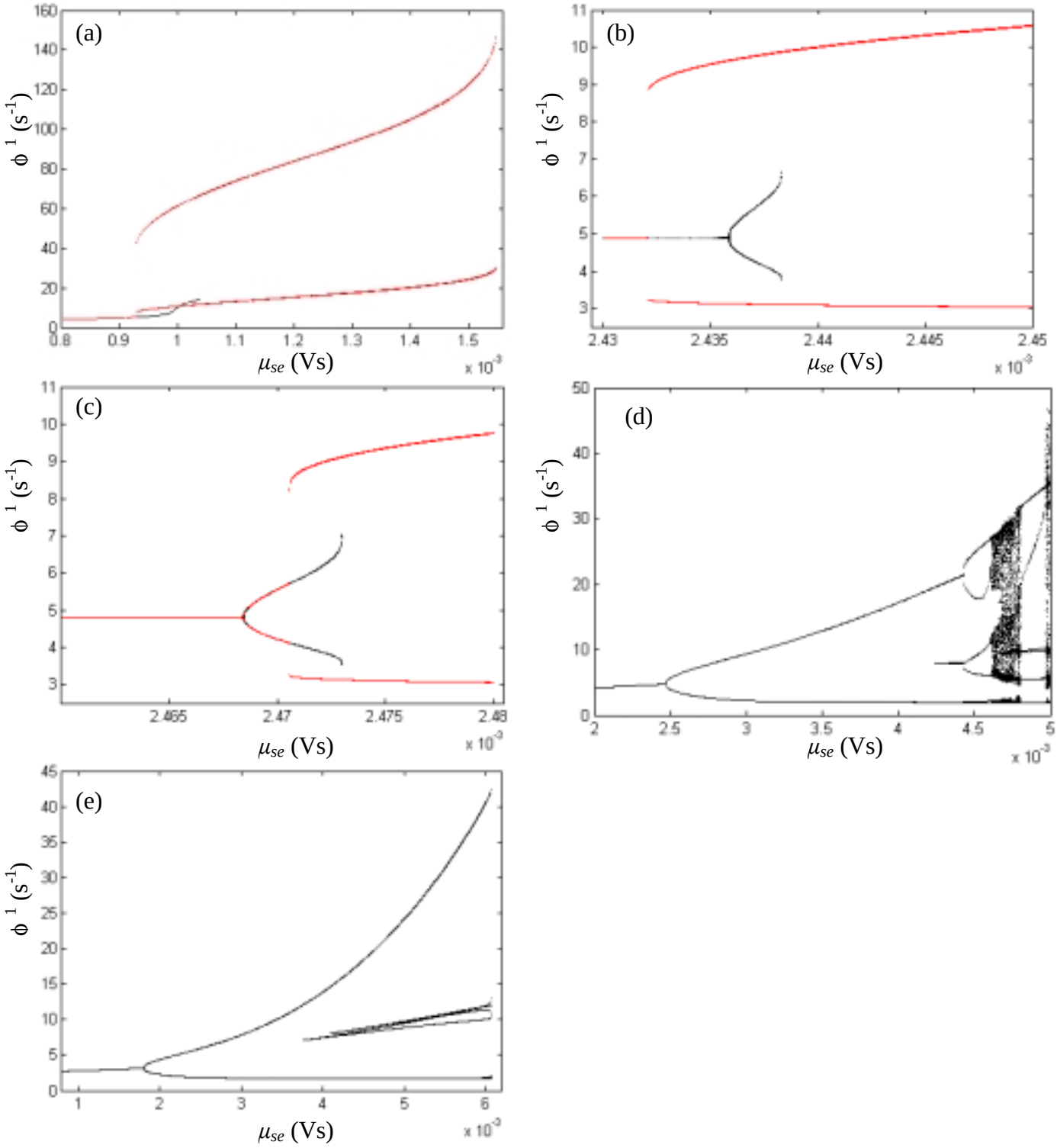

Breakspear, *et al.* (2005)

Figure 10

Table 1

Quantity	Value for Absence Seizure	Value for Tonic-Clonic Seizure	Unit	Meaning
Q_{max}	250	250	s^{-1}	Maximum firing rate
□	15	15	mV	Mean neuronal threshold
σ	6	6	mV	Threshold variability
γ_e	100	100	s^{-1}	Ratio of conduction velocity to mean range of axons
α	50	60	s^{-1}	Inverse rise time of membrane
β	200	240	s^{-1}	Inverse decay time of potential
t_0	80	80	ms	Corticothalamic return time (complete return loop)
μ_{ee}	1.0	1.2	mV s	Excitatory cortico-cortical gain
$-\mu_{ei}$	1.8	1.8	mV s	Inhibitory corticocortical gain
μ_{es}	3.2	1.4	mV s	Specific thalamic nuclei to cortical gain
μ_{se}	4.4	1.0	mV s	Cortical to specific thalamic nuclei gain
$-\mu_{sr}$	0.8	1.0	mV s	Thalamic reticular nucleus to specific thalamic nucleus gain
$\mu_{sn}\phi_n$	2.0	1.0	mV s	Nonspecific subthalamic input onto specific thalamic nuclei
μ_{re}	1.6	0.2	mV s	Excitatory cortical to thalamic reticular nucleus gain
μ_{rs}	0.6	0.2	mV s	Specific to reticular thalamic nuclei gain

Breakspear, *et al.* (2005)

Table 1